Simulation of Summer Diurnal Circulations over the Northwest United States

Matthew C. Brewer[1]

Clifford F. Mass

Department of Atmospheric Sciences
University of Washington, Seattle, Washington

[1]Corresponding author, Matthew C. Brewer, Department of Atmospheric Sciences, University of Washington, Box 351640, Seattle, Washington 98195-164045, email: mcbrewer83@yahoo.com

Abstract

During the summer, strong surface heating combines with the terrain and land/water contrasts of the northwest U.S. to create a complex array of diurnal circulations. Though observational and modeling studies have described some of these circulations, advances in high-resolution numerical modeling allow for a more comprehensive and three-dimensional examination.

In order to simulate typical summer conditions over the Pacific Northwest, three-hourly GFS model output for July and August 2009-2011 was used to initialize and provide boundary conditions for a high-resolution WRF model run. To ensure the realism of the simulation, it was compared to observations on a collection of days representing typical summer conditions. Generally, it was found that the simulated diurnal wind, relative humidity, and temperature were close to observations.

It is shown that regional diurnal circulations occur on a number of interacting scales, ranging from upslope/downslope winds on local terrain features to larger-scale circulations such as between the Pacific Ocean and the western Oregon and Washington interiors or between the eastern and western sides of the Cascades. Such multi-scale diurnal circulations occur simultaneously, with the interactions producing complex structures, several of which are described in this paper. Locations such as the Strait of Juan de Fuca and downstream of the major Cascade Mountain gaps reach maximum wind speeds between 2100-2400 LDT, while most other areas have peak winds earlier in the day. Localized nocturnal low-level wind maxima are described, including one over the northern Willamette Valley and another over the high plateau of eastern Oregon.

1. Introduction

The timing, intensity, and evolution of diurnal winds, and their influence on other meteorological variables are important for aviation, wind energy, agriculture, and boating, among other applications. Fire managers must be familiar with the diurnal meteorology of wildfire areas before making critical decisions that affect life and property, and an understanding of diurnal winds sheds light on regional variations in air quality and the transport of pollutants.

Thermally induced diurnal circulations are created when surface radiative forcing interacts with variations in topography and land-water contrasts. These circulations are amplified in summer when solar insolation is strongest and land-water temperature differences are generally greatest. The summer season is also characterized by fewer synoptic systems, less clouds, and reduced snow in the mountains, leading to strengthening of the diurnal winds.

The terrain of the northwest United States, its proximity to the Pacific Ocean, and the large amount of coastline in the region produce complex diurnal wind circulations on many scales. The most significant terrain feature of the region is the Cascade Range, with a crest approximately 100-200 km inland from the coast (Figure 1). Elevations in the Cascade Range reach 2500-3000 m, with higher volcanic peaks. Significant topographic features west of the Cascades include the Olympic Mountains, the Puget Sound lowlands, the Willamette Valley, and the Coast Range. The Columbia Basin lies in eastern Washington while the Oregon Plateau is found in eastern Oregon with elevations of ~1000 m.

To illustrate average summer conditions over the region, Weather Research and Forecasting (WRF) model output at 12-km grid spacing and averaged over July and August

2009-2011 is shown in Figure 2[1]. During this period, the eastern Pacific Ocean is dominated by the Pacific High, which drives northerly flow and ocean upwelling along the coast. Such northerly flow is particularly strong along the southern Oregon (Elliot and O'Brian 1977; Bielli el al. 2002) and northern California coasts (Zemba and Friehe 1987; Holt 1996; Burk and Thompson 1996; Taylor et al. 2008), with little change in strength during the day. As the heat low over the Great Basin strengthens during the day while high pressure is maintained offshore, the low-level geopotential height gradient builds over the Cascades. The Cascades impede marine air from reaching the east side, making the interior substantially warmer than the western lowlands. The contrasting thermal conditions across the Cascades are demonstrated in Figure 3 by histograms of daily high temperatures for July and August 2007-2012 at KSEA (Seattle-Tacoma Airport, WA) and HHMS (Hanford, WA). Most summer days in Seattle reach 65-85ºF while at Hanford, on the east side of the mountains, temperature maxima are more frequently between 85 and 105ºF, roughly 20ºF warmer.

Terrain features such as the Strait of Juan de Fuca, Olympic Mountains, Chehalis Gap, Puget Sound, and Cascade Mountains result in complex diurnal circulations over western Washington. Staley (1957) used hodographs from July and August for three years to describe the diurnal winds over the Puget Sound region. Southerly or light/variable winds in the morning are replaced by northerly flow (known as the *Sound Breeze*) in the afternoon. Staley found that stations east of the Puget Sound have a maximum westerly component in the early afternoon hours and a maximum easterly component at night due to regional mountain/valley and sea/land breeze circulations. Mass (1982) used vector-averaged winds from July for three years and

[1] For several years, the University of Washington Department of Atmospheric Sciences has run the WRF model at 36-, 12-, 4-, and 1.3-km grid spacing. More information is found at http://www.atmos.washington.edu/mm5rt/info.html.

found that westerlies blow through the Strait of Juan de Fuca the entire day, reaching a maximum in the evening. He found that divergence occurs over the Puget Sound in the afternoon and convergence during the night from diurnal mountain breezes on the slopes of the Olympic and Cascade Mountains, consistent with the results of Staley (1957).

Staley (1959) examined diurnal winds over eastern Washington's Columbia Basin and found outflow during the day and inflow at night. Ellensburg, on the eastern slopes of the Cascades, has a maximum wind from the northwest at 1800 Local Daylight Time (LDT), while at Yakima and Hanford, south and southeast of Ellensburg respectively, strong northwest winds occur a few hours later. Staley attributed these northwesterly winds to a combination of cooler air coming through the gaps in the Cascades and local drainage flows. Doran and Zhong (1994) used observations and simulations to describe these strong northwesterly winds, suggesting that they develop as the inland thermal low develops, drawing in cooler air from west of the Cascades. As heating subsides during the evening, the cooler air coming through Snoqualmie Pass accelerates down the eastern slopes (katabatic flow) and is channeled by the terrain.

Though the synoptic pattern shown in Figure 2, with a synoptic high offshore and a thermal low centered over the Great Basin, is dominant in the summer, there are other transient synoptic regimes that occur during the summer. Periods of low-level easterly (offshore) flow develop as upper-level ridges move over the region and high surface pressure builds inland (Mass 1986; Chien et al. 1997; Brewer et al. 2012). During these periods, under a continental rather than marine influence, western Oregon and Washington experience their warmest weather. Often following easterly flow events, coastally trapped southerlies move northward along the West Coast behind the northward extension of a coastal thermal trough, resulting in a marine push and onshore flow (Mass et al. 1986; Mass and Bond 1996; Nuss 2000). Less frequent

synoptic evolutions include the development of a weak offshore trough or the approach of a weak front, both of which contribute to coastal southerly flow.

Although the aforementioned literature provides insights into diurnal winds over the Pacific Northwest, the three-dimensional structures and temporal evolutions of important regional diurnal circulations are not well documented. Fortunately, improvements in the resolution and physics of numerical models allows for more accurate and comprehensive simulations of such diurnal circulations. Furthermore, there are several important regional diurnal circulations that have not been investigated, such as the mesoscale diurnal flows of eastern Oregon.

This paper describes an approach for simulating climatological summer conditions over the Pacific Northwest and applies this technique to enhance knowledge of northwest U.S. diurnal circulations. Specifically, a high-resolution simulation is used to examine the differing scales of diurnal circulations over the Pacific Northwest and their three-dimensional structures, evolutions, and mutual interactions.

2. Model description

For this research, NOAA/NWS Global Forecast System (GFS) model output at one-degree latitude/longitude resolution was obtained for July and August 2009-2011. These data were averaged by hour, and the resulting files were used to initialize and provide boundary conditions for a high-resolution WRF (version 3.5) model run. An outer nest of 36-km grid spacing was used, along with three one-way nested domains of 12-, 4-, and 4/3-km grid spacing (Figure 4). The 4/3-km run was primarily used in this analysis. Thompson microphysics, RRTMG long-wave and short-wave radiation schemes, the Yonsei boundary layer scheme, 38

vertical full-sigma levels, MODIS land use, and a model top of 50 hPa were used in this simulation. The Simplified Arakawa-Schubert cumulus parameterization was applied in the outer three domains, but no cumulus parameterization was used for the 4/3 km-domain.

The model was initialized at 1700 LDT, corresponding to 0000 UTC, and was run for 48 hours. A 24-hour period for forecast hours 12 to 35 (0500 LDT to 0400 LDT) was used to describe the diurnal cycle over the region. The reason for initializing the model at 1700 LDT is twofold. First, sufficient spin-up time is needed to produce realistic conditions. Second, if the model is initialized at night, the low-resolution GFS initialization/boundary conditions will not resolve thermal structures in the lower troposphere produced by surface heating the prior day. This is particularly true near complex terrain.

3. Verification

The goal of the WRF model run is to simulate typical summer (July and August) diurnal wind, temperature, and moisture variations. In order to verify the accuracy of the model simulation, it was compared to observations from a collection of days with typical summer synoptic conditions. The question is how to define objectively a "typical" summer day. Figure 5 shows histograms of wind direction for five spatially distributed stations for July and August 2009-2011 at the hour of the climatological maximum wind speed at each station using 10° direction bins[1]. Each station has a well-defined mode of wind direction at the time of their respective climatological maximum wind. The most frequently occurring wind direction, as well as adjacent directions with more than five days, is identified (colored red) in each histogram in Figure 5. Days outside of the mode are colored blue. Only those days within the mode (red) at

[1] For each station in Figure 5, there are a few days when the wind speed is zero and hence would have no wind direction; those days are not represented in this figure.

all five stations were used for comparison against the WRF run. Specifically, 54% of the days (100 of 186 days) remained after the filtering was applied.

There are some differences among these five stations in the percentage of days characterized by the mode. For example, buoy 46050 (Figure 5), just offshore of central Oregon, has a narrow mode encompassing about 75% of the days. There is a secondary maximum for southerly to southwesterly winds associated with coastally trapped wind reversals and the occasional trough passage. Four other stations—KELN (Ellensburg, WA), KDLS (The Dalles, OR), CWQK (southern tip of Vancouver Island), and KHQM (Hoquiam, WA)—have dominant winds from the west to northwest, with higher percentages of days within the mode. Easterly-flow events are evident at KELN on the eastern slopes of the Cascades, where a secondary maximum is found.

A map of the observations that were used for comparison against the WRF run is shown in Figure 6. The selected stations are distributed throughout the region and are high-quality aviation reporting sites. Fourteen of the stations are from the Automated Surface Observing System (ASOS), while one station (CWQK) is from Environment Canada. Since CWQK does not have temperature and relative humidity, nearby KLCM (Port Angeles, WA) was used in place of CWQK for those variables.

Figure 7 shows a comparison of model wind speed (green) to the scalar-average observed wind speed (blue) as well as the 16^{th} and 84^{th} percentiles (red) from observations. The observational average and 16^{th} and 84^{th} percentiles were calculated using the filtered summer days (54% of total days) from July and August 2009-2011 as described above. Figure 8 shows model wind direction (green) compared to the average wind direction at that station (blue), calculated by averaging the zonal (u) and meridional (v) components.

In general, model winds are highly realistic. Along the coast, simulated winds are close to observed, though winds are ~2 m s^{-1} stronger than observed late in the forecast period at KHQM and KONP, with a wind direction error of ~20º at KHQM. At KAST, model winds are marginally weaker than observed in the evening and early morning, though the model wind direction matches observations closely for the full 24-hour period. The model wind speeds and timing of the strong northwesterly winds in the Strait of Juan de Fuca are highly realistic as shown by the wind speed and direction at CWQK (Figures 7 and 8).

Over the western interior, KSEA (Seattle-Tacoma Airport) observed and modeled wind directions turn from westerly to northerly between afternoon and evening, and model wind speeds are weaker than observed by about 1 m s^{-1}. At night, when the winds are weak, there is less agreement. In the Willamette Valley, model-simulated northwesterly winds at KVUO and KEUG are close to observed, and the moderate northerly flow that occurs during the afternoon and evening on the east side of the Cascade Mountains near KBDN (Bend, OR) is reproduced well. Despite the complex terrain surrounding KDLS and KELN, the intensity and timing of the peak wind at both KELN and KDLS closely match observations. Further east, model winds at KALW (Walla Walla, WA), KGEG (Spokane, WA), and KBKE (Baker City, OR) resemble average summer diurnal winds at these stations. Finally, model winds at KLMT (Klamath Falls, OR) are close to the observational average.

Figure 9 shows model-simulated 10-meter winds over northwestern Washington at 1800 LDT compared to a figure from Mass 1982 that shows the observed average wind vectors at the same time. As observed, the model simulation shows northerly flow of about 4-7 m s^{-1} over the central Sound, along with westerly (easterly) flow on the east (west) of the Sound. Furthermore, there is strong westerly flow in the Strait of Juan de Fuca in both simulated and observed wind

fields. South of the Olympic Mountains, moderate westerlies (4-6 m s^{-1}) prevail in the Chehalis Gap in both the simulated and observed maps.

The WRF run simulates realistically the diurnal temperature cycle over the region (Figure 10). Near the coast, where the diurnal range is reduced by the influence of the Pacific, the model accurately simulates the temperature evolution. At KCLM, in the Strait of Juan de Fuca, the model temperatures are higher than observed by about 2-3 °C for most of the forecast period. Simulated temperatures away from the coast are realistic. Simulated morning temperatures at KBKE are 4-5 °C warmer than observed, though model daytime temperatures are much closer to observed.

Generally, most stations, especially away from the coast, manifest a diurnal cycle in relative humidity that resembles observations (Figure 11). Along the coast, model relative humidity is higher than observed by about 5-15% for KUIL, KHQM, KAST, and KONP. Relative humidity in the Willamette Valley reaches a minimum earlier in the afternoon than observed (see KPDX and KEUG), and this deficiency also appears at a few stations east of the Cascade crest (KELN and KDLS). The model relative humidity east of the Cascades is more realistic than on the west side, with the exception of the morning hours at KBKE, where model temperatures did not cool sufficiently in the morning.

4. Results

A. 2-m temperature and relative humidity

The 4/3-km simulations of 925 hPa geopotential height, 10-m wind, and 2-m temperature every six hours (forecast hour 12, 18, 24, and 30) are presented in Figure 12. High pressure dominates offshore and lower pressure occurs inland, especially at 1700 LDT, due to strong solar

heating east of the Cascades. As a result, the pressure gradient across the Cascades increases during the daytime hours. Some of the daytime heating is still evident at 2300 LDT, particularly over the basin of eastern Washington and the eastern Oregon highlands.

The diurnal range of 2-meter temperature over the forecast period (12-35 hours into the simulation, 0500 to 0400 LDT) is shown in Figure 13. The range, which varies from 1 to 20 °C, was calculated by subtracting the minimum temperature from the maximum temperature at each grid point over the simulated diurnal period. Offshore and coastal areas have little variation in temperature, as do higher terrain locations, such as in the Cascades, Olympics and Coast Range. Low-lying areas that are shielded from the influence of the ocean have a large range in temperature such as the Willamette Valley, the interior southwest Washington, and areas east of the Cascade crest such as the Oregon Plateau and the Columbia Basin.

The diurnal variations in temperature and wind have a profound effect on relative humidity over the region. The simulated evolution of 2-m relative humidity over the Northwest is shown in Figure 14. At 0500 LDT, dry conditions occur east of the Cascades, while much higher relative humidity occurs over the Pacific and the western lowlands. There are limited areas east of the Cascades where relative humidity values are greater than 50%, such as the eastern Columbia Basin and south-central Oregon near Klamath Falls. At 1100 LDT, relative humidity lowers at most locations due to surface heating except for the western slopes of the Cascade Mountains, where upslope flow leads to higher values. At 1700 LDT, most areas have lower relative humidity values except for the Cascade crest and the tops of the Olympics. Converging daytime upslope flow often leads to cumulus convection and enhanced relative humidity near the crests of the Cascade, Olympic and Coastal Mountains during the summer. At 2300 LDT and into the morning hours (0500 LDT), most areas have an increase in relative

humidity as surface temperatures cool. An interesting exception is the tops of the Olympic Mountains and portions of the north Cascades where relative humidity drops dramatically between 1700 and 0500 LDT as the upslope flow weakens and reverses.

Figure 15 shows the range of simulated 2-m relative humidity over the region. Central Oregon has the highest range of relative humidity (50% and more). This large range is confirmed in observations at KBDN in Bend, Oregon (Figure 6 shows location) and near the Oregon/California boarder at KLMT in Klamath Falls, Oregon (63%.). Coastal relative humidity varies little, as proximity to the ocean keeps temperatures and relative humidity stable. Mountain slopes tend to have a small range in relative humidity, while western inland areas away from water (Willamette Valley, lower Columbia Basin) have larger ranges.

B. 10-m wind

The evolution of 10-m wind over the region using the WRF simulation is found in Figure 16. Offshore, winds increase by 1-3 m s^{-1} during the day, remaining northerly or northwesterly throughout the diurnal cycle. Over the Strait of Juan de Fuca, the winds are weakest at 1100 LDT, although still moderately strong at 5-6 m s^{-1} from the northwest. The Strait winds reach a peak at ~2200 LDT with northwesterly wind speeds at 12-13 m s^{-1}. Over the western interior of Oregon and Washington, winds are generally weakest at 0500-0800 LDT. Westerlies associated with the Pacific Ocean sea breeze pass through the gaps in the coastal mountains during the day, reaching a peak near 1700 LDT, and weaken during the evening and overnight. In the Willamette Valley, winds are weak in the morning, with northwest to north winds strengthening in the afternoon and evening, reaching a peak of 3-6 m s^{-1} around 2000 LDT before weakening during the night.

Westerlies coming through the Columbia River Gorge, the only sea-level gap through the Cascade Mountains, reach a maximum between 1700 and 2000 LDT. However, winds extending out of Snoqualmie and Stevens passes into central Washington reach a maximum between 2000 and 2300 LDT. Over the western Columbia Basin, winds are light in the morning and reach a maximum in the late evening as westerlies rush down the eastern slopes of the Cascades.

Weak southwesterly upslope flow forms in the late morning over the eastern Columbia Basin at 1100 LDT and continues into the afternoon and evening. Over the Oregon Plateau, winds are weak in the morning hours. Northwesterly upslope flow strengthens over north-central Oregon between 1400 and 1700 LDT and is strongest in the southern portion of the plateau at 2000-2300 LDT.

Figure 17 shows the hour at which the maximum 10-m wind is reached for each grid point over Oregon and Washington, with a terrain map for easy reference. The most common colors are blues, purples, and pinks, indicating maximum winds during the afternoon or evening. Lighter blues, which are mostly found on mountain slopes, such as on the eastern slopes of the Olympic Mountains or limited areas on the western slopes of the Cascades, indicate maximum winds during the early afternoon hours, consistent with upslope flow. Darker blues indicate that peak winds occur in late afternoon and are found offshore and along the western slopes of the Coastal and Cascade Mountains. The winds over the lowland areas near Puget Sound and in the Willamette Valley, as well as a large part of eastern Oregon, peak around 2000-2100 LDT, as indicated by purple and pink. Finally, reds indicate maxima around 2200-2400 LDT over the eastern Strait of Juan de Fuca, the lower Columbia Basin and on some of the eastern Oregon highlands. Interestingly, an area of green color (0600-1000 LDT) is found over a portion of eastern Washington, which is consistent with a local maximum at KPUW (Pullman, WA; not

shown), though winds are slightly stronger at KPUW in the late afternoon. Also, there is little diurnal variation of wind speed (~1 m s^{-1}) at KPUW and KGEG.

Figure 18 shows the diurnal range of the u (top) and the v (bottom) components of the 10-m wind. West of the Cascades, most of the variation in the u component is over the eastern Strait of Juan de Fuca and the central Strait of Georgia. In western Oregon, there is a moderate range (4-8 m s^{-1}) in the u component within the gaps of the Coast Range. Over the Puget Sound, there is a moderate range in the v-wind component from the Sound Breeze, with weak southerlies in the morning and moderate northerlies in the afternoon. There is little variation in the 10-m v component offshore, despite speeds of greater than 10 m s^{-1} over the coastal waters of southern Oregon.

The largest variations in both components, up to 12 m s^{-1} in some areas, occur east of the Cascades. In the morning, weak easterly upslope flow develops on the eastern slopes of the Washington Cascades. Westerly winds of 6-10 m s^{-1} develop in the evening, thus explaining the large range in the u component in that area. There is also a large variation (6-12 m s^{-1}) in the u and v components in eastern Oregon, due to strong nighttime downslope flow into the Snake River Valley in Idaho. In central Oregon, there is a large variation (6-10 m s^{-1}) in the v component as northerlies develop during the day and reverse to weak southerlies at night. This diurnal variation is verified by observations at Bend, Oregon (Figures 7 and 8).

C. Lower-tropospheric wind

To provide a three-dimensional view of the evolution of the regional diurnal circulations, Figure 19 shows winds at 975, 925, 875, and 825 hPa, with no winds shown if the terrain is

above the pressure level shown. Over the coastal waters, winds are relatively constant in time at all levels, with speed decreasing with height.

In contrast, over the western lowlands of Oregon and Washington, the winds vary substantially in time at all levels. At 1400 LDT, winds are from the north to northwest over western Oregon and Washington and weaken with height. These winds increase in the evening at lower levels and remain weak at 825 hPa. Interestingly, several locations over the Willamette Valley and over the Chehalis Gap (immediately south of the Olympics) develop strong winds at night aloft (975-925 hPa), reaching a peak at 2300 LDT. Winds in the lower troposphere over the Strait of Juan de Fuca reach a maximum at 2000-2300 LDT, with the strongest westerlies at 975 hPa.

In the Cascades, strong westerlies develop in the afternoon within the gaps such as the Columbia River Gorge and the Stampede/Snoqualmie Pass gap. Near and east of the gap exits, winds strengthen during the evening and reach a maximum near 2300 LDT, well after the hours of peak heating.

A major feature in the simulations, yet not discussed in previous literatures, is the diurnal northerly flows over the highlands of eastern Oregon. Upslope flow is evident on the slopes of the higher terrain in north-central Oregon at 1700 LDT at 925, 875, and 825 hPa. At 2000 LDT, northerlies at 825 hPa strengthen dramatically and move southward, and strengthen further at 2300 LDT, after which winds weaken into the morning hours. Interestingly, this feature is barely noticeable at the surface (Figure 16).

To determine whether the diurnal northerly flow over the Oregon Plateau is realistic, the wind speed and direction at two stations on the Plateau were compared to the model simulations (Figure 20). These sites are at the top of mountain peaks about 1500 feet above the plateau floor

and are Remote Automated Weather Stations (RAWS) run by the Bureau of Land Management and the U.S. Forest Service. Both observations and the model simulations show maximum wind speed between 2100 and 2300 LDT, and the observed wind direction agrees closely with the model during the period of strongest winds.

To further analyze the three-dimensional structure of the regional wind features, vertical cross sections were created, and the locations are shown in Figure 21. Figure 22 shows cross sections over the northernmost portion of the Willamette Valley at 1600 and 2200 LDT. At 1600 LDT, potential temperatures indicate a mixed layer up to ~900 hPa, and weak to moderate northwesterly winds throughout the lower atmosphere. Six hours later, northwesterly lower-tropospheric winds strengthen dramatically as the daytime boundary layer collapses and stability increases at the surface.

To evaluate the realism of these changes over the northern Willamette Valley, observations from the Aircraft Communications and Reporting System (ACARS) for aircraft landing/taking off from the Portland International Airport (PDX) were examined for typical summer days as defined earlier (Table 1). Winds are weak below 1000 m during the afternoon of 21 July 2011, while during the evening, aircraft measured a low-level jet max of 10 m s^{-1} at 435 m above ground. During the afternoon of 29 July 2011, low-level winds were again weak and uniform but strengthened that evening to 10 m s^{-1} around 600 m. Reviewing ACARS data for many days and over several summer seasons revealed that an evening wind maximum is a common feature in the summer over Portland, Oregon, thus confirming the model simulation.

East-west cross sections of the simulated wind and thermal fields over Washington State at two different times are shown in Figure 23; the cross section location is shown in Figure 21. At 1600 LDT, northerly flow and stable conditions are evident off the coast of Washington, with

a strong horizontal temperature gradient over the coastal region. Daytime boundary layer mixing over western Washington appears to prevent stronger winds over the coastal lowlands despite the large temperature gradient. Six hours later, during the evening (2200 LDT), more stable conditions prevail over the lowest 50 hPa of western Washington and strong northwesterlies develop with the stable layer. At this time there is still a modest temperature gradient over the coastal lowlands.

Over the Cascade crest, moderate westerlies occur at 1600 LDT in the presence of a strong temperature gradient between the west and east sides of the barrier. Weak winds and a well-mixed boundary layer exist east of the Cascades. Six hours later, strong westerly downslope winds were evident over the eastern slopes of the Cascades, where substantial low-level cooling has occurred. Data from a 400-foot tower at Hanford, WA confirms the realism of the simulated downslope westerly flow, with a wind maximum occurring on average at 2300 LDT (not shown).

5. Discussion and summary

During the summer, strong surface heating combines with the terrain and land/water contrasts of the northwest U.S. to create diurnal circulations that develop and interact on a variety of scales. This paper provides a three-dimensional description of these complex diurnal circulations over the Pacific Northwest, making use of high-resolution simulations. For this work, National Weather Service GFS model output (three-hourly) was averaged for July and August 2009-2011 and used for initial and boundary conditions in a WRF model run. This simulation was examined to explore the three-dimensional evolution of winds, temperature, and relative humidity over the region for a typical summer diurnal period.

To analyze the validity of the simulation, the WRF model run was compared to a collection of days with typical summer conditions. Wind direction at five stations was used to filter out summer days with atypical synoptic conditions, leaving 54% of the available 186 days (from July and August 2009-2011) to compare to the WRF simulation. It was found that the model simulations produced realistic diurnal variations in wind speed, wind direction, relative humidity, and temperature.

The summer synoptic environment over the northwest U.S. has a large impact on the mesoscale diurnal variations over the region. The East Pacific High produces northerlies along the coast and cool coastal sea-surface temperatures from upwelling, and pushes cool, marine air into the western lowlands. During the day, pressure lowers east of the Cascades as daytime solar heating enhances the east-west pressure gradient, particularly across the Cascade Mountains (Figure 12). This gradient contributes to afternoon and early evening westerlies over the coastal lowlands and within Cascade Mountain gaps.

West of the Cascades, 10-m wind simulations show that sea breeze westerlies reach a maximum intensity near 1700 LDT, particularly within the gaps of the Coast Range, such as the Chehalis Gap south of the Olympic Mountains. Within the Willamette Valley, north-to-northwesterly flow develops and is enhanced in the afternoon by westerlies pushing inland from the coast, reaching a peak near 1900 LDT. In the Puget Sound region, simulations confirm studies by Mass (1982) and Staley (1957), which show moderate northerly flow in the afternoon and weakening at night. Within the Strait of Juan de Fuca, strong terrain-channeled northwesterly flow occurs throughout the day, reaching a maximum in the evening near 2200 LDT.

Within the Cascades, westerly flow near the surface through the near sea-level Columbia River Gorge is strongest between 1700 and 2000 LDT. In contrast, the Gorge winds at ~925 hPa are stronger later in the evening (2000-2300 LDT). An evening wind maximum is also apparent for the downslope wind maximum east of the Snoqualmie and Stevens Passes in Central Washington. Doran and Zhong (1994) described the strong northwesterly winds rushing down the eastern slopes of the Cascades as a combination of katabatic flow and cooler air coming through from the west side through the pass.

The WRF simulations and confirming observations showed that evening wind maxima occur above the surface over the northern Willamette Valley and the Chehalis Gap, reaching maximum strength near 2300 LDT at approximately 975 hPa. These low-level wind maxima are reminiscent of low-level nocturnal jets/wind maxima that occur all over the world (Revelle and Nilsson 2008; Baas et al. 2009; Kairpot et al. 2009; Kumar 2012), and it has been shown that the WRF model can realistically simulate these wind phenomena (Storm and Basu 2010; Michelson et al. 2010; Colle and Novak 2010). During the day, horizontal winds often weaken in the boundary layer due to the vertical mixing of air slowed by surface drag. As the surface cools during the evening, a low-level inversion forms, inhibiting vertical motion and decoupling the lower troposphere from the surface. Such a decoupling from surface drag allows existing pressure/temperature gradients to accelerate the wind to form low-level wind maxima (Arya 2001), and such evening gradients were evident in the simulations (Figure 23).

In the case of the well-documented low-level jet in the Great Plains, as well as other larger-scale nocturnal low-level jets over relatively flat terrain, there is a balance between friction, the Coriolis force, and the pressure gradient force within the boundary layer during the day. In the evening as the near-surface inversion forms, the loss of friction results in an inertial

oscillation that drives supergeostrophic low-level winds (Markowski and Richardson 2010). However, due to the smaller scale of the low-level wind features over the Willamette Valley and Chehalis Gap and their relative short longevity, the Coriolis force is small and thus accelerations of the wind are primarily due to the pressure gradient force.

Over the Oregon Plateau, the simulations indicated moderate northerly flow during the evening. These winds are hardly noticeable at the surface, but are found immediately aloft (lowest 50 hPa) above the surface with wind speeds near 10-12 m/s. Such Oregon plateau northerlies are confirmed by observations at the tops of local mountain peaks. It appears that this northerly flow is driven by strong temperature/pressure gradients that develop during day and which are able to accelerate low-level flow during the evening as drag lessens as increased stability decouples the lower atmosphere from the surface.

An important aspect of the diurnal winds over the region is that diurnal circulations of various scales interact simultaneously over the region, producing a complex and highly three-dimensional flow and thermal evolution. There are local sea breeze circulations between the Pacific Ocean and the coastal lowlands, regional sea breeze winds between the western Washington interior land mass and the cool waters of the Straits of Georgia and Juan de Fuca, diurnal circulations between the inland bodies of water and surrounding land, and slope flows on the substantial terrain of the region. There are also diurnal circulations between the interior of eastern Washington and the western Washington lowlands, between the heated interior and the Pacific Ocean, and regional diurnal flows over the eastern Oregon Plateau. Even more complexity is produced by the varying stability that results in a diurnal cycle of coupling/decoupling of the free atmosphere with air near the surface, influenced by surface drag and diabatic effects. The skill of modern high-resolution modeling systems in generally

duplicating these complex, three-dimensional diurnal circulations is a testament to improvements in modeling systems during the past decades.

This paper described the large-scale wind features over the Pacific Northwest, and also briefly discussed the individual wind features over the region, such as in the Strait of Juan de Fuca, and the Columbia River Gorge. Further analysis is needed to discover the forcing mechanisms and specific synoptic conditions that drive each wind feature, as well as a description of their average intensity and evolution. Individual case studies would be useful to further explore the model's ability to simulate these wind features.

Acknowledgments

This research was supported by the USDA Forest Service.

References

Arya, S. P., 2001: *Introduction to Micrometeorology, Second Edition*. Academic Press, 418 pp.

Baas, P., F. C. Bosveld, H. K. Baltink, and A. A. M. Holtslag, 2009: A climatology of nocturnal low-level jets at Cabauw. *J. Appl. Meteor. Climatol.*, **48**, 1627-1642.

Bielli, S., P. Barbour, R. Samelson, E. Skyllingstad, and J. Wilczak, 2002: Numerical study of the diurnal cycle along the central Oregon coast during summertime northerly flow. *Mon. Wea. Rev.*, **130**, 992-1008.

Brewer, M. C., C. F. Mass, and B. E. Potter, 2012: The West Coast Thermal Trough: Climatology and synoptic evolution. *Mon. Wea. Rev.*, **140**, 3820-3843.

Burk, S. D., and W. T. Thompson, 1996: The summertime low-level jet and MBL structure along the California coast. *Mon. Wea. Rev.*, **124**, 668-686.

Chien, F. C., C. F. Mass, and Y. H. Kuo, 1997: Interaction of a warm-season frontal system with the coastal mountains of the western United States. Part I: Prefrontal onshore push, coastal ridging, and alongshore southerlies. *Mon. Wea. Rev.*, **125**, 1705-1729.

Colle, B. A., and D. R. Novak, 2010: The New York Bight Jet: Climatology and dynamical evolution. *Mon. Wea. Rev*., **138**, 2385-2404.

Doran, J. C., and S. Zhong, 1994: Regional drainage flows in the Pacific Northwest. *Mon. Wea. Rev.*, **122**, 1158-1167.

Elliott, D. L., and J. J. O'Brien, 1977: Observational studies of the marine boundary layer over an upwelling region. *Mon. Wea. Rev.*, **105**, 86-98.

Holt, T. R., 1996: Mesoscale forcing of a boundary layer jet along the California coast. *J. Geophys. Res.*, **101**, 4235-4254.

Karipot, A., M. Y. Leclerc, and G. Zhang, 2009: Characteristics of nocturnal low-level jets observed in the north Florida area. *Mon. Wea. Rev.*, **137**, 2605-2621.

Kumar, M. S., V. K. Anandan, T. N. Rao, and P. N. Reddy, 2012: A climatological study of the nocturnal boundary layer over a complex-terrain station. *J. Appl. Meteor. Climatol.*, **51**, 813-825.

Markowski, P., and Y. Richardson, 2010: *Mesoscale Meteorology in Midlatitudes*. John Wiley & Sons, 407 pp.

Mass, C. F., 1982: The topographically forced diurnal circulations of western Washington State and their influence on precipitation. *Mon. Wea. Rev.*, **110**, 170-183.

Mass, C. F., M. D. Albright, and D. J. Brees, 1986: The onshore surge of marine air into the Pacific Northwest: A coastal region of complex terrain. *Mon. Wea. Rev.*, **114**, 2602-2627.

Mass, C. F., and N. A. Bond, 1996: Coastally trapped wind reversals along the United States west coast during the warm season. Part II: Synoptic evolution. *Mon. Wea. Rev.*, **124**, 446-461.

Michelson, S. A., I. V. Djalalova, and J. Bao, 2010: Evaluation of the summertime low-level winds simulated by MM5 in the Central Valley of California. *J. Appl. Meteor. Climatol*., **49**, 2230-2245.

Nuss, W. A., and Coauthors, 2000: Coastally Trapped Wind Reversals: Progress toward understanding. *Bull. Amer. Meteor. Soc.*, **81**, 719-743.

Olsson, L. E., W. P. Elliott, and S. Hsu, 1973: Marine air penetration in western Oregon: An observational study. *Mon. Wea. Rev.*, **101**, 356-362.

ReVelle, D. O., and E. D. Nilsson, 2008: Summertime low-level jets over the high-latitude Arctic Ocean. *J. Appl. Meteor. Climatol.*, **47**, 1770-1784.

Staley, D. O., 1957: The low-level sea breeze of northwest Washington. *J. Meteor*., **14**, 458-470.

Staley, D. O., 1959: Some observations of surface-wind oscillations in a heated basin. *J. Meteor*., **16**, 364-370.

1 Storm, B., and S. Basu, 2010: The WRF model forecast-derived low-level wind shear
2 climatology over the United States Great Plains. *Energies*, **3**, 258-276.
3
4 Zemba, J., and C. A. Friehe, 1987: The marine boundary layer jet in the coastal ocean dynamics
5 experiment. *J. Geophys. Res.*, **92**, 1489-1496.

Tables

July 21, 2011

Flight 9940

Time (LDT)	Lat (°)	Lon (°)	Ht (m)	P (mb)	Dir (°)	Spd (m/s)
14:00	45.59	-122.59	42	1008	158	3
14:00	45.60	-122.60	208	988	163	5
14:00	45.60	-122.62	455	960	189	5
14:01	45.61	-122.65	678	934	205	4
14:01	45.62	-122.68	921	907	223	4
14:01	45.63	-122.69	1079	890	216	4

Flight 9921

Time (LDT)	Lat (°)	Lon (°)	Ht (m)	P (mb)	Dir (°)	Spd (m/s)
20:24	45.59	-122.59	57	1006	345	6
20:24	45.60	-122.60	233	986	352	6
20:25	45.60	-122.61	435	962	336	10
20:25	45.60	-122.62	548	949	326	9
20:25	45.61	-122.64	705	931	296	5
20:26	45.62	-122.67	954	904	272	5

July 29, 2011

Flight 9919

Time (LDT)	Lat (°)	Lon (°)	Ht (m)	P (mb)	Dir (°)	Spd (m/s)
16:07	45.59	-122.59	70	1005	331	4
16:08	45.60	-122.60	203	989	350	5
16:08	45.60	-122.62	390	967	337	4
16:08	45.61	-122.64	540	950	343	5
16:09	45.62	-122.68	892	911	338	5
16:09	45.63	-122.70	1166	881	347	6

Flight 9895

Time (LDT)	Lat (°)	Lon (°)	Ht (m)	P (mb)	Dir (°)	Spd (m/s)
21:05	45.59	-122.59	14	1012	338	3
21:05	45.60	-122.61	346	972	347	9
21:06	45.61	-122.65	593	944	359	10
21:06	45.61	-122.66	725	929	7	8
21:07	45.63	-122.70	995	899	23	5
21:07	45.64	-122.73	1285	868	352	3

Table 1: ACARS data for 4 flights in July 2011.

Figure Caption List

Figure 1: The terrain and major geographical features of the northwest U.S.

Figure 2: Average 925 hPa geopotential height (m, contours), temperature (°C, color shading) (left), and 10-m wind (vectors and color shading) (right) from WRF model output for July-August 2009-2011.

Figure 3: Histograms of daily maximum temperatures for July and August 2007-2012 at Seattle-Tacoma Airport and Hanford, Washington.

Figure 4: Domains for the WRF model simulations.

Figure 5: Histograms of wind direction for July and August 2009-2011 at the time of the climatological maximum wind speed (noted at the top of each graph) for a collection of regional observing sites. The percentage of days within the primary mode (red color) is shown.

Figure 6: Map of stations used for verification.

Figure 7: Comparison of model wind speed (green) to observed average (blue) and 16^{th} and 84^{th} percentiles (red).

Figure 8: Comparison of model (green) and observed (blue) wind direction.

Figure 9: Vector-average surface wind for three years in July (from Mass 1982, top) and 10-m wind speed from the WRF simulation (vectors and color shading, bottom) valid at 1800 LDT.

Figure 10: Comparison of model temperature (green) to the observed average (blue) and 16^{th} and 84^{th} percentiles (red).

Figure 11: Comparison of model relative humidity (green) to observations (blue) and the 16^{th} and 84^{th} percentiles (red).

Figure 12: 925 hPa geopotential height (black contours), temperature (color shading, °C), and wind (full barb = 5 m s^{-1}).

Figure 13: Diurnal range of 2-m temperature (°C).

Figure 14: Evolution of 2-m relative humidity from the WRF run.

Figure 15: Range of RH in % at 2 m.

Figure 16: 10-m simulated wind (colors and vectors).

Figure 17: Hour at which the maximum wind is reached (LDT, left), and terrain height (meters, right).

Figure 18: Diurnal range of 10-m u (top) and v (bottom) wind components.

Figure 19: Wind (colors and vectors) with terrain above the pressure level blocked out.

Figure 20: Comparison of model (green) and observational (blue) wind speed and direction. Wind speeds shown as in Figure 7.

Figure 21: Locations of cross sections for Figures 22 (short yellow line) and 23 (long yellow line).

Figure 22: Wind (colors and barbs, full barb = 5 m s^{-1}) and potential temperature (blue lines, °K) from the 4/3-km WRF simulation for 1600 (left) and 2200 (right) LDT.

Figure 23: Wind (colors and barbs, full barb = 5 m s^{-1}) and potential temperature (blue lines, °K) on the left, and temperature (°C) on the right from the 4/3-km WRF simulation.

Figure 1: The terrain and major geographical features of the northwest U.S.

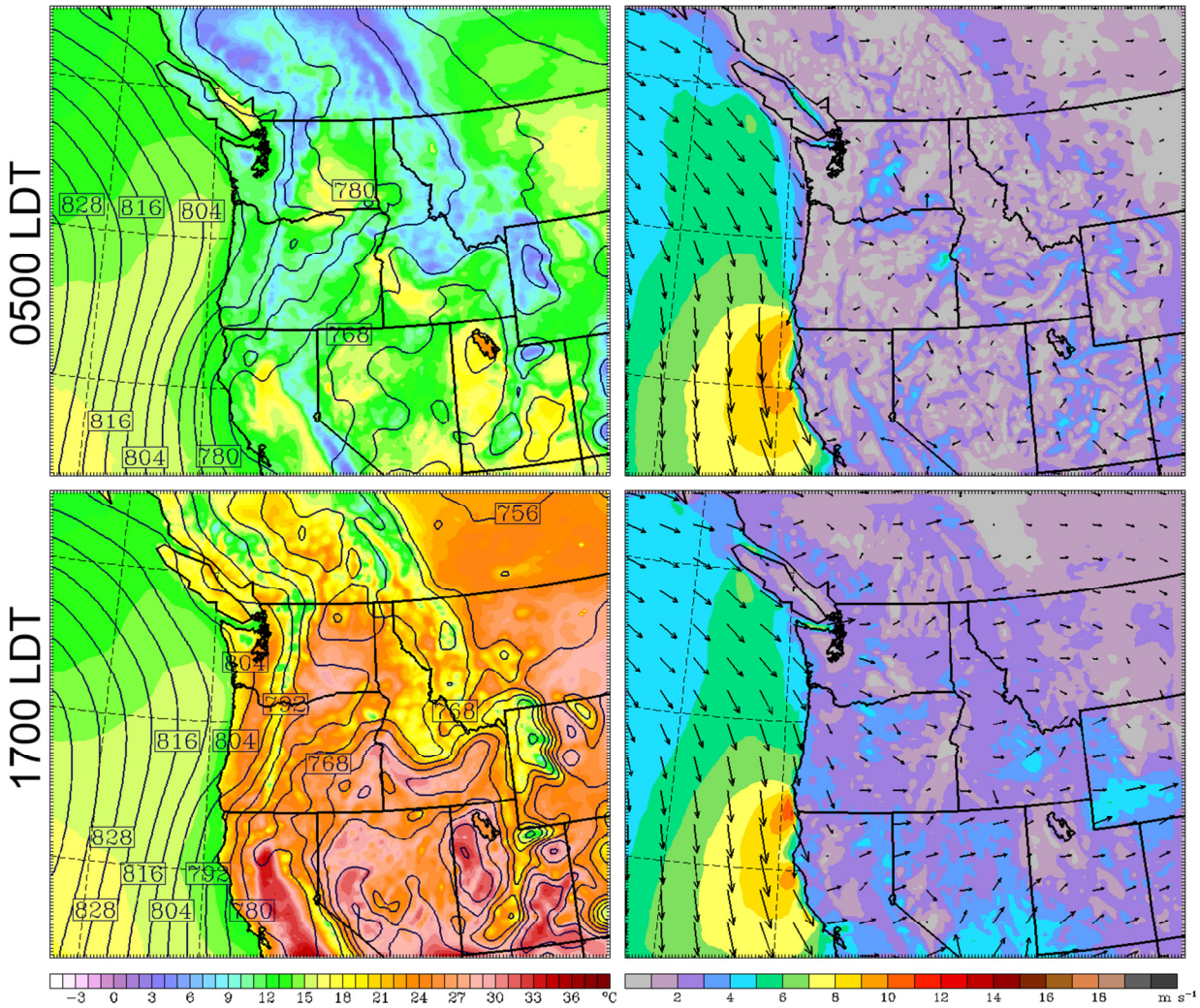

Figure 2: Average 925 hPa geopotential height (m, contours), temperature (°C, color shading) (left), and 10-m wind (vectors and color shading) (right) from WRF model output for July-August 2009-2011.

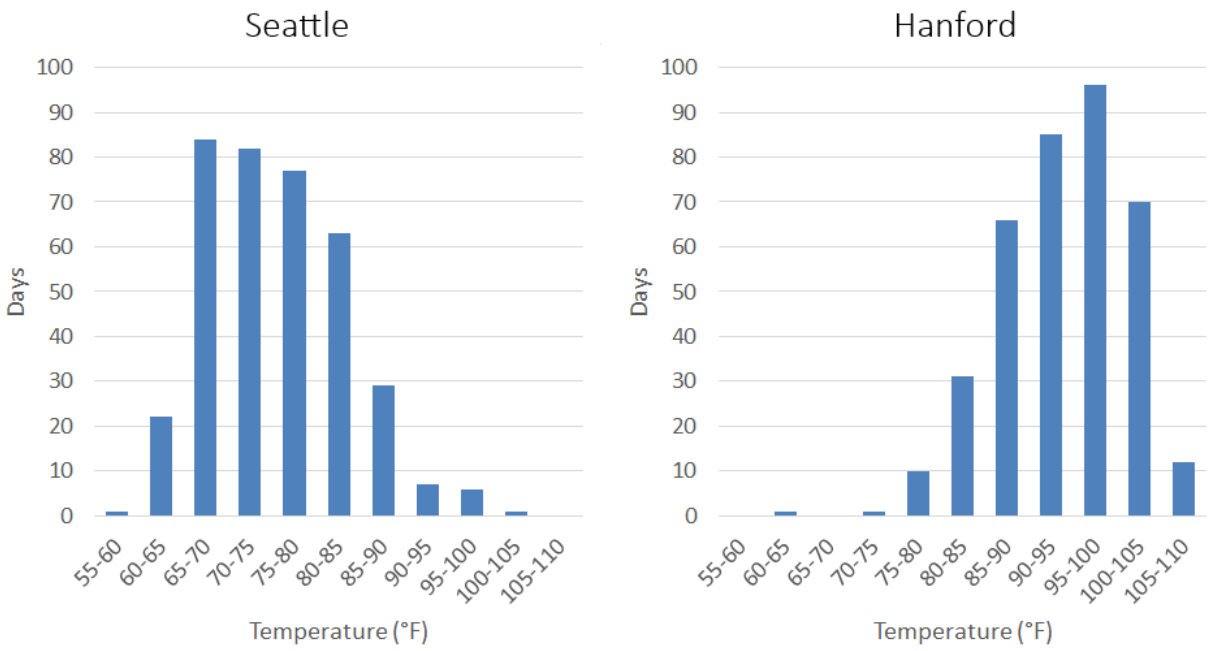

Figure 3: Histograms of daily maximum temperatures for July and August 2007-2012 at Seattle-Tacoma Airport and Hanford, Washington.

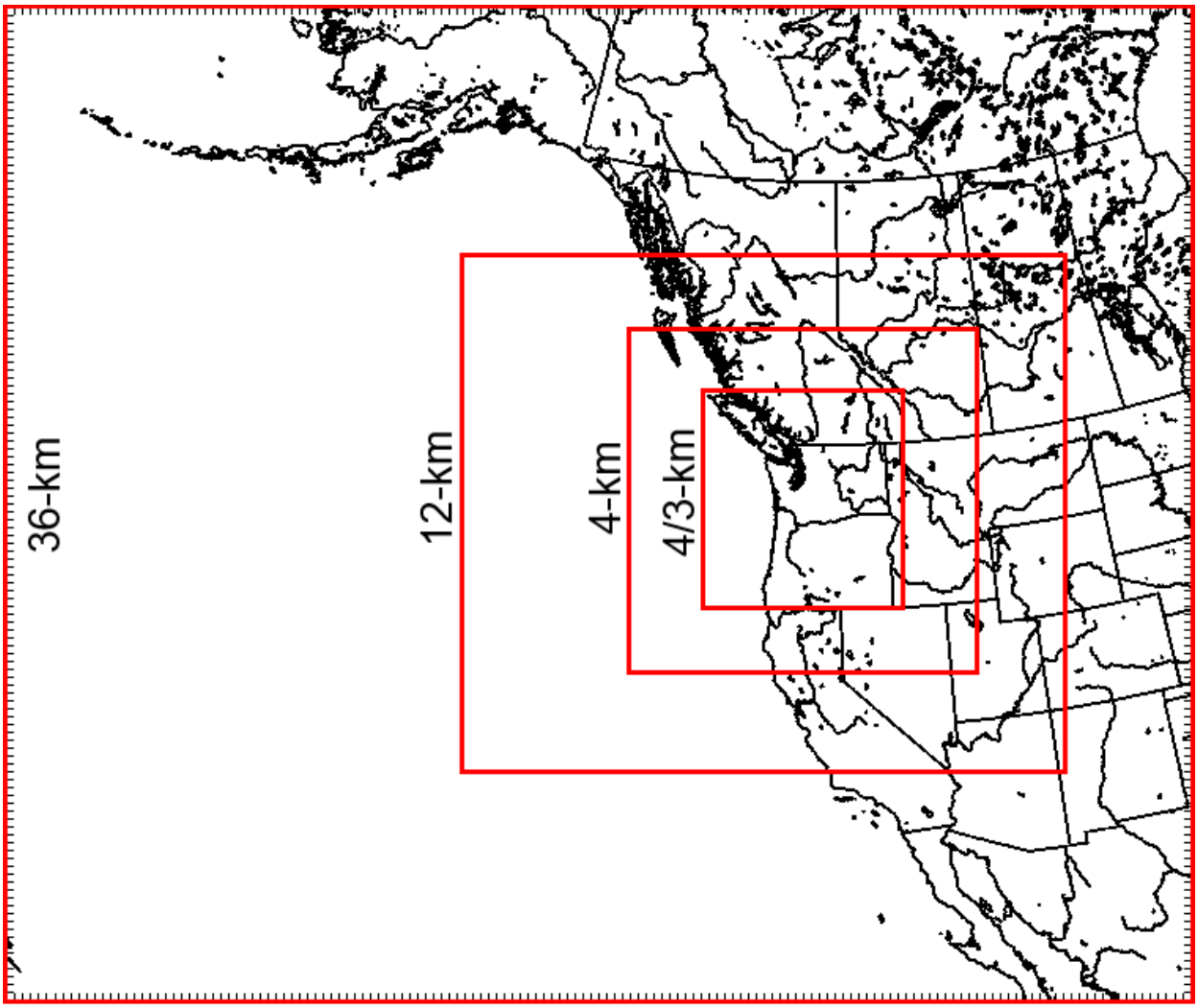

Figure 4: Domains for the WRF model simulations.

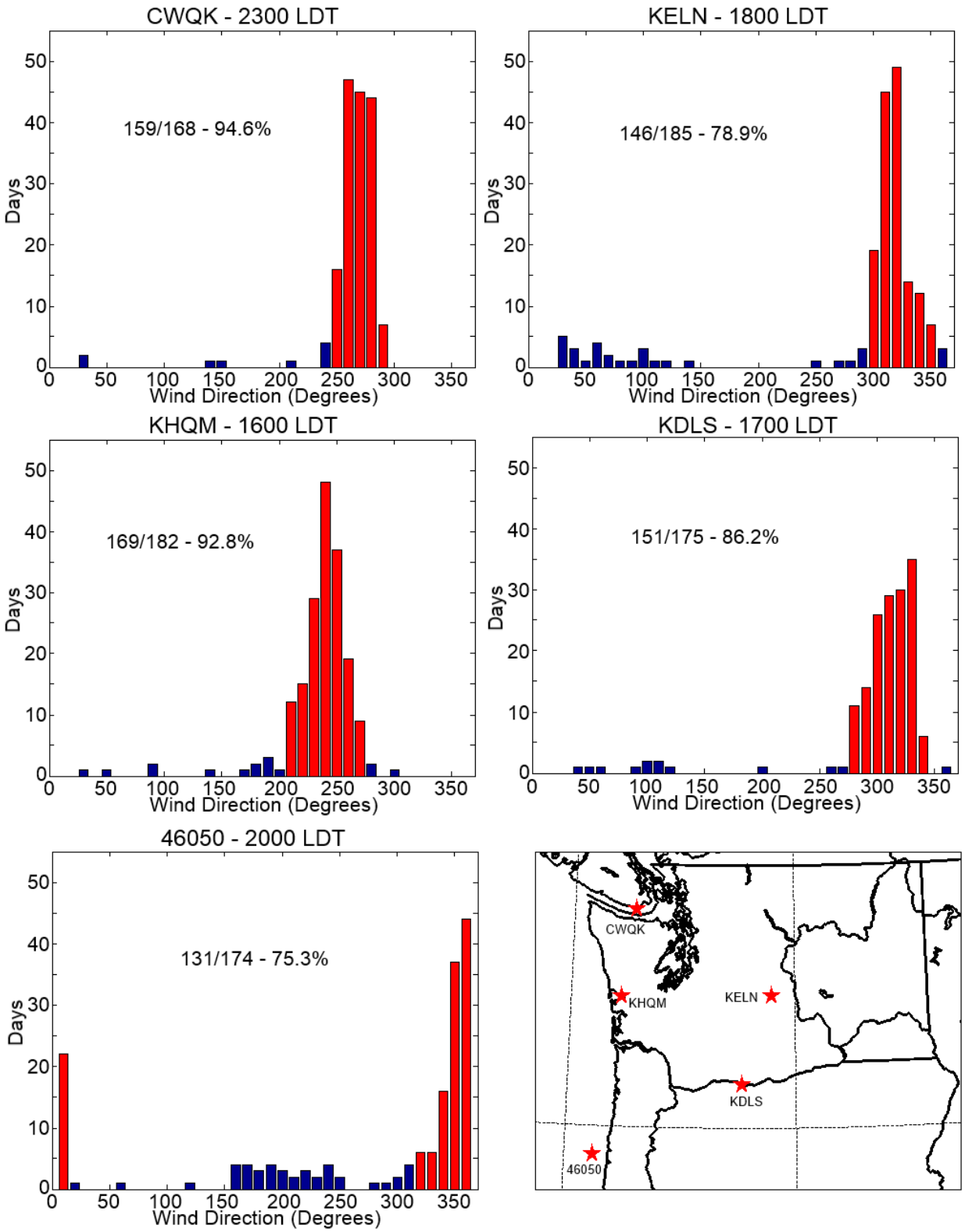

Figure 5: Histograms of wind direction for July and August 2009-2011 at the time of the climatological maximum wind speed (noted at the top of each graph) for a collection of regional observing sites. The percentage of days within the primary mode (red color) is shown.

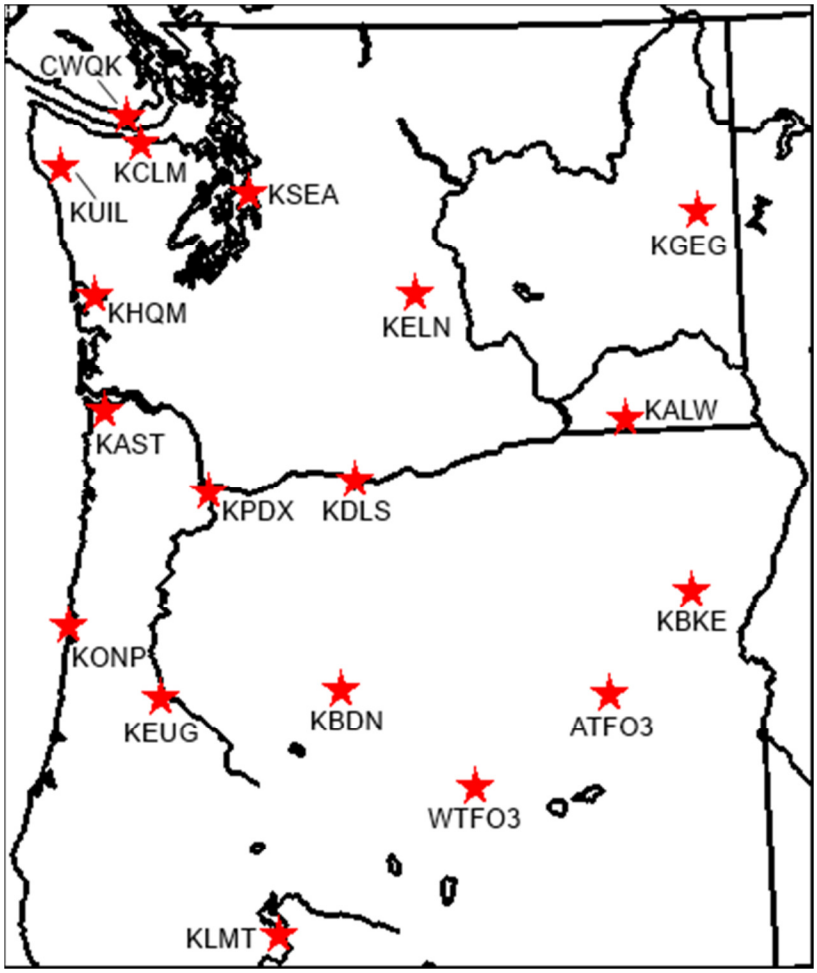

Figure 6: Map of stations used for verification.

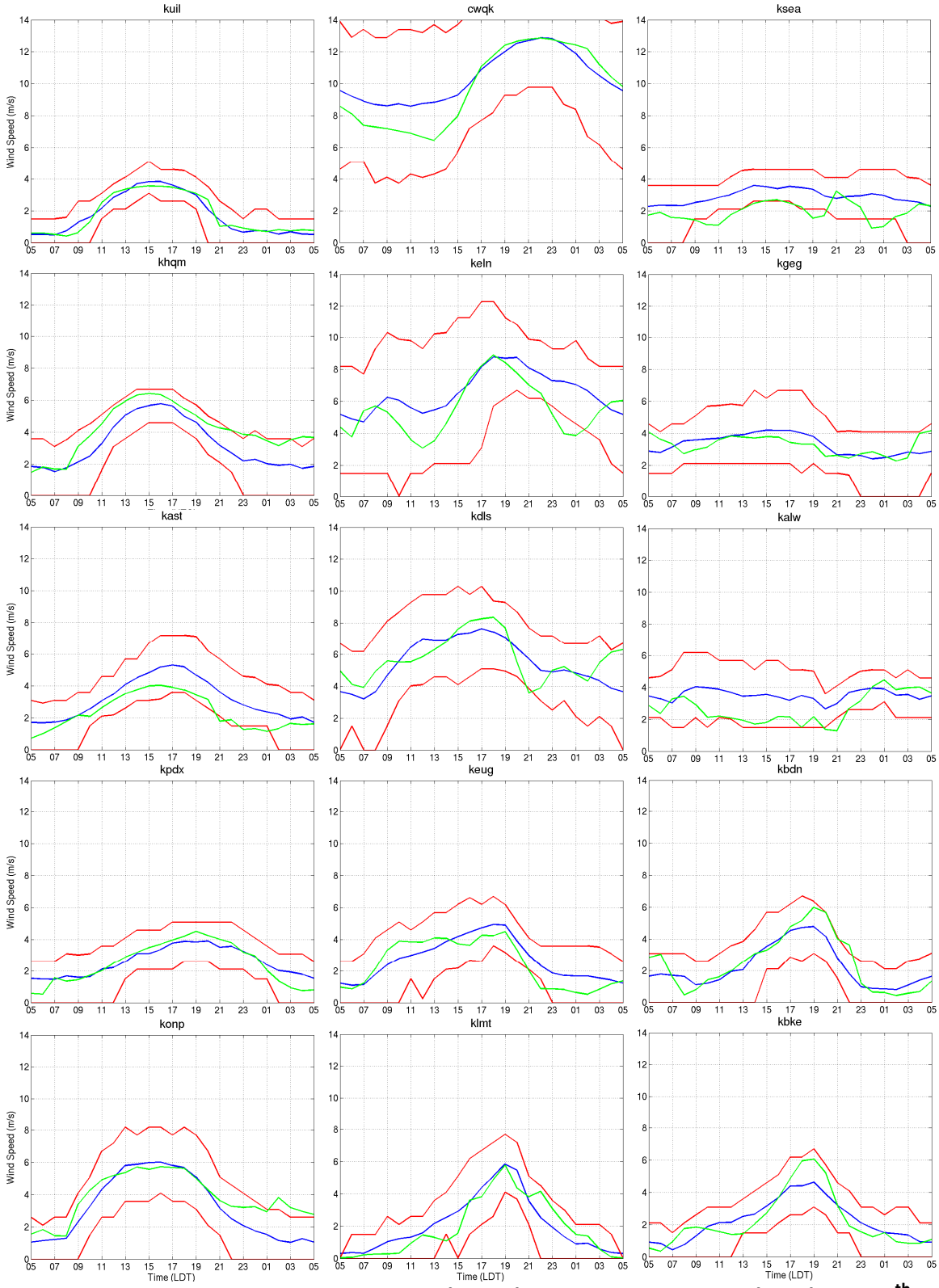

Figure 7: Comparison of model wind speed (green) to observed average (blue) and 16th and 84th percentiles (red).

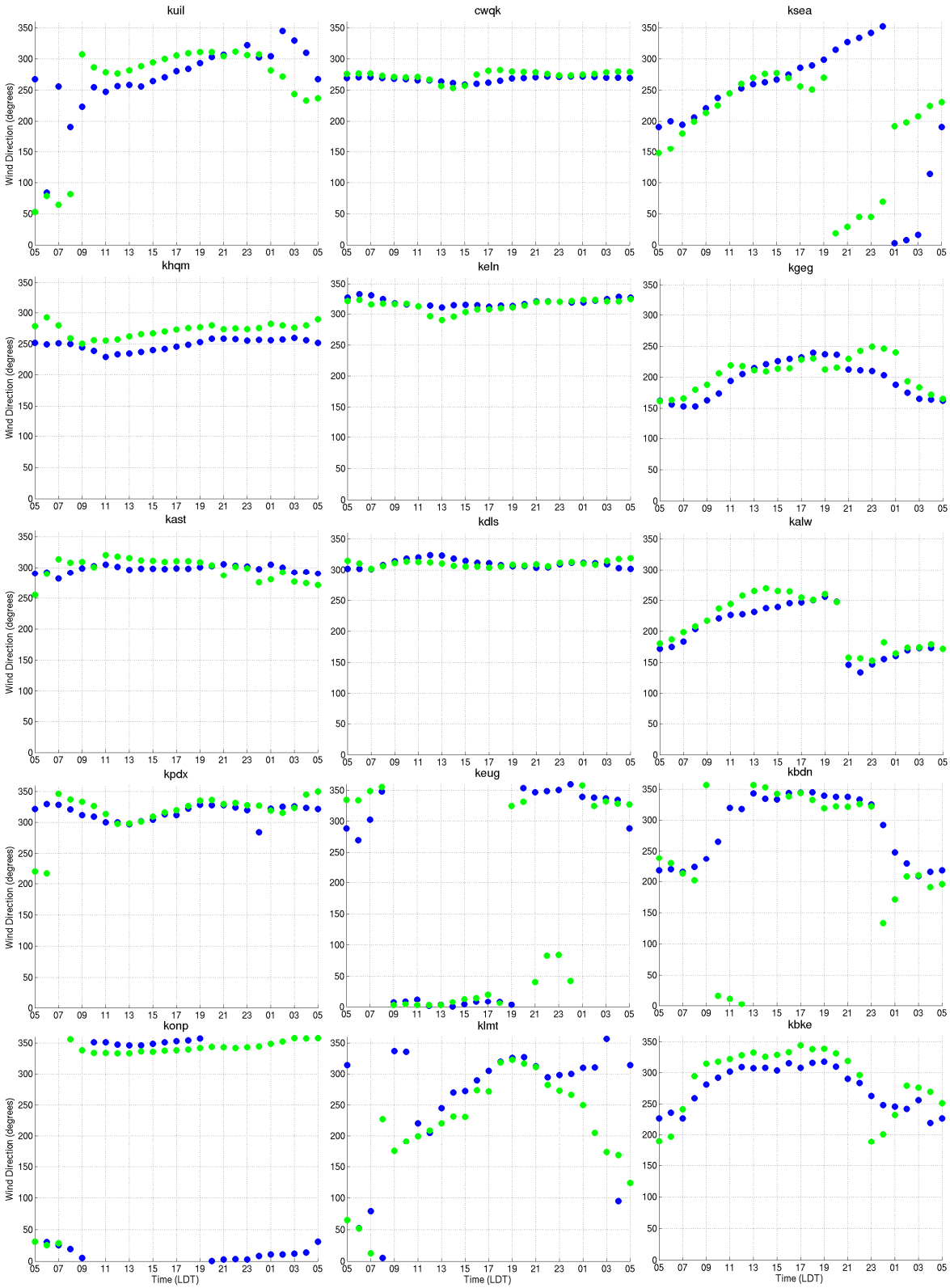

Figure 8: Comparison of model (green) and observed (blue) wind direction.

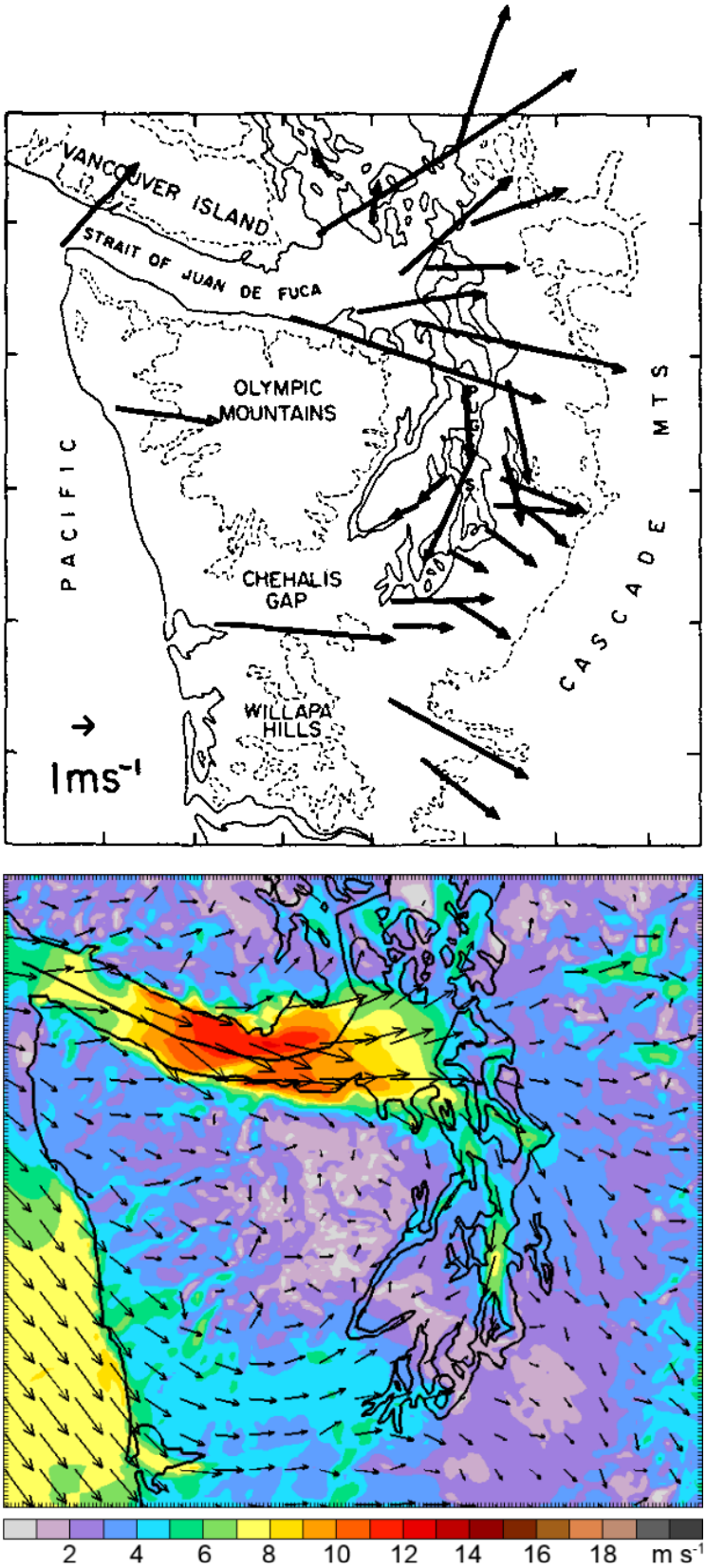

Figure 9: Vector-average surface wind for three years in July (from Mass 1982, top) and 10-m wind speed from the WRF simulation (vectors and color shading, bottom) valid at 1800 LDT.

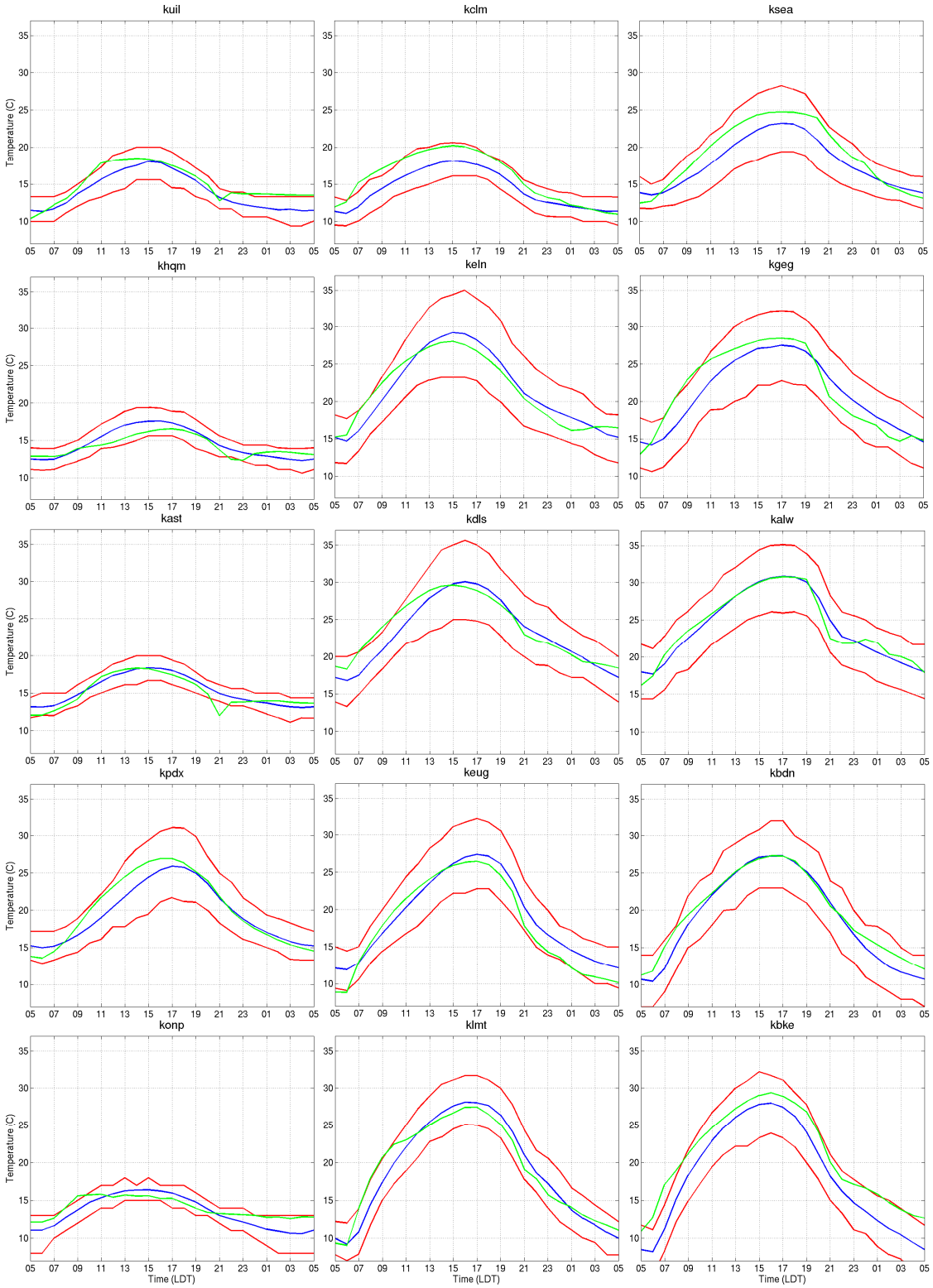

Figure 10: Comparison of model temperature (green) to the observed average (blue) and 16th and 84th percentiles (red).

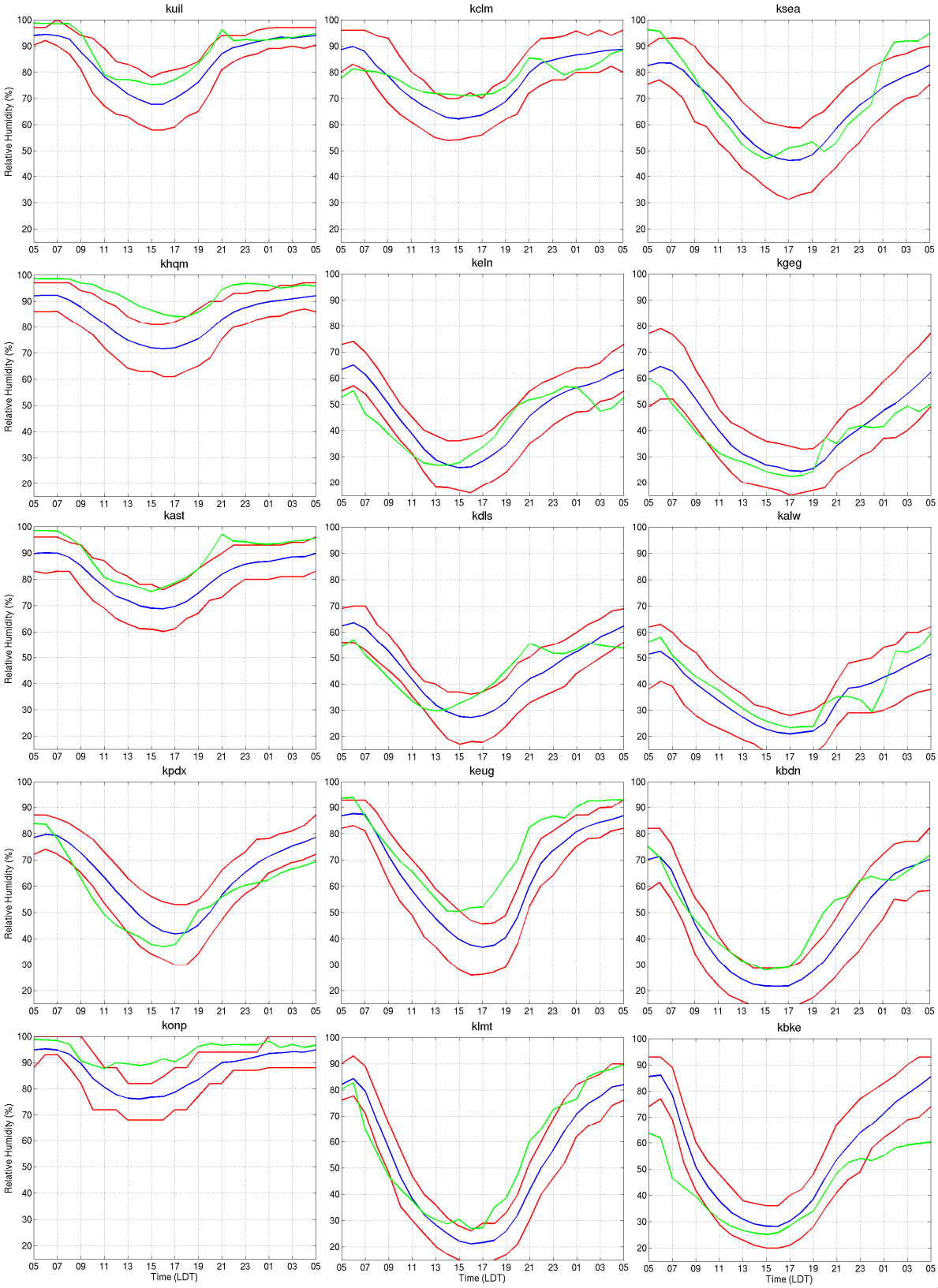

Figure 11: Comparison of model relative humidity (green) to observations (blue) and the 16th and 84th percentiles (red).

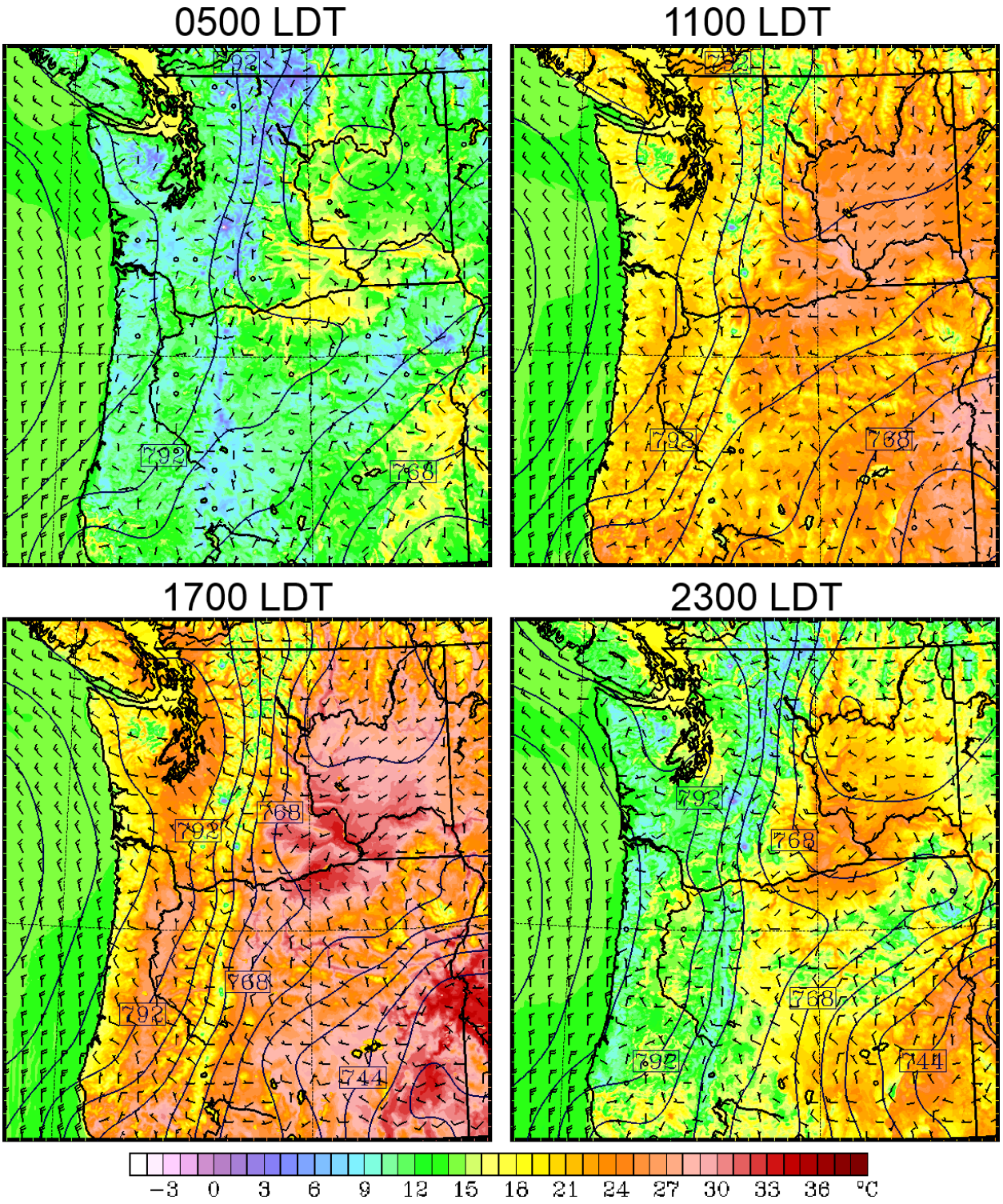

Figure 12: 925 hPa geopotential height (black contours), temperature (color shading, °C), and wind (full barb = 5 m s^{-1}).

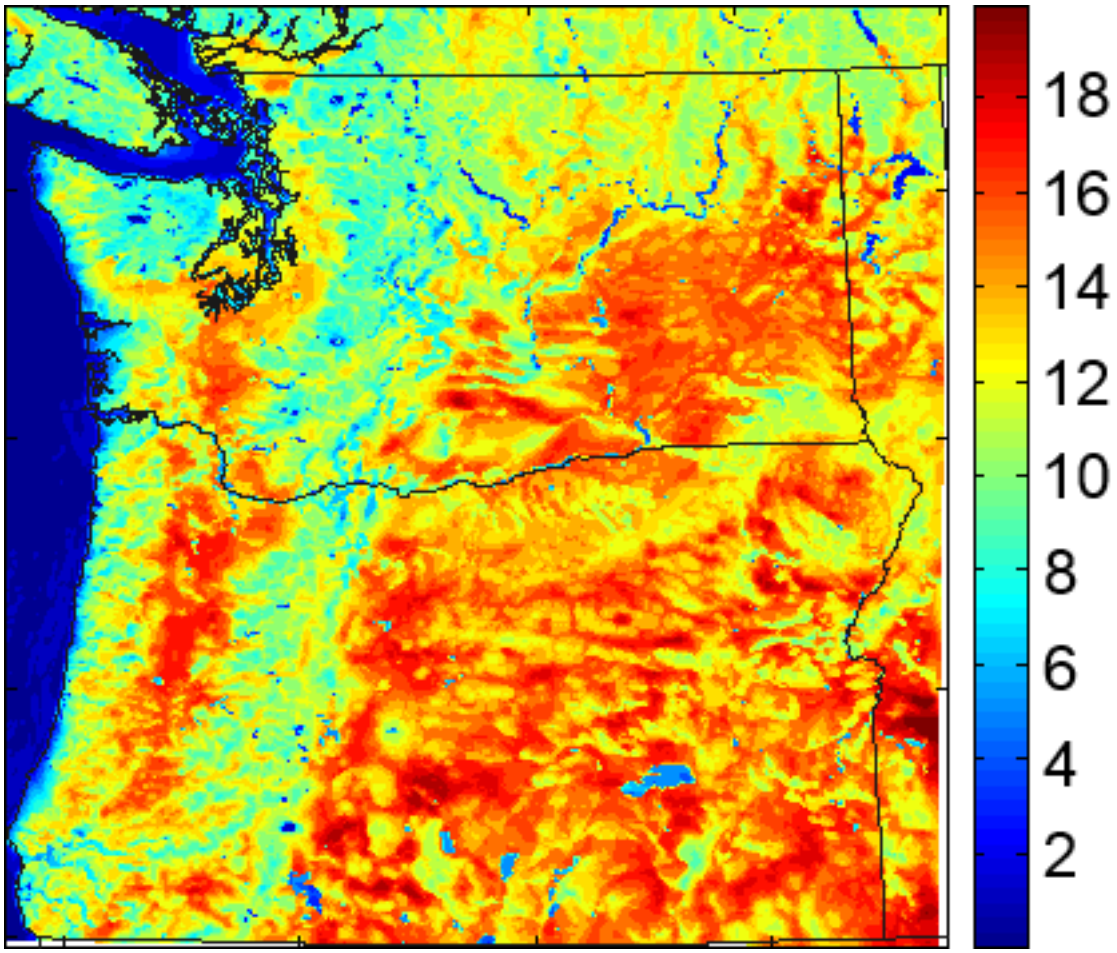

Figure 13: Diurnal range of 2-m temperature (°C).

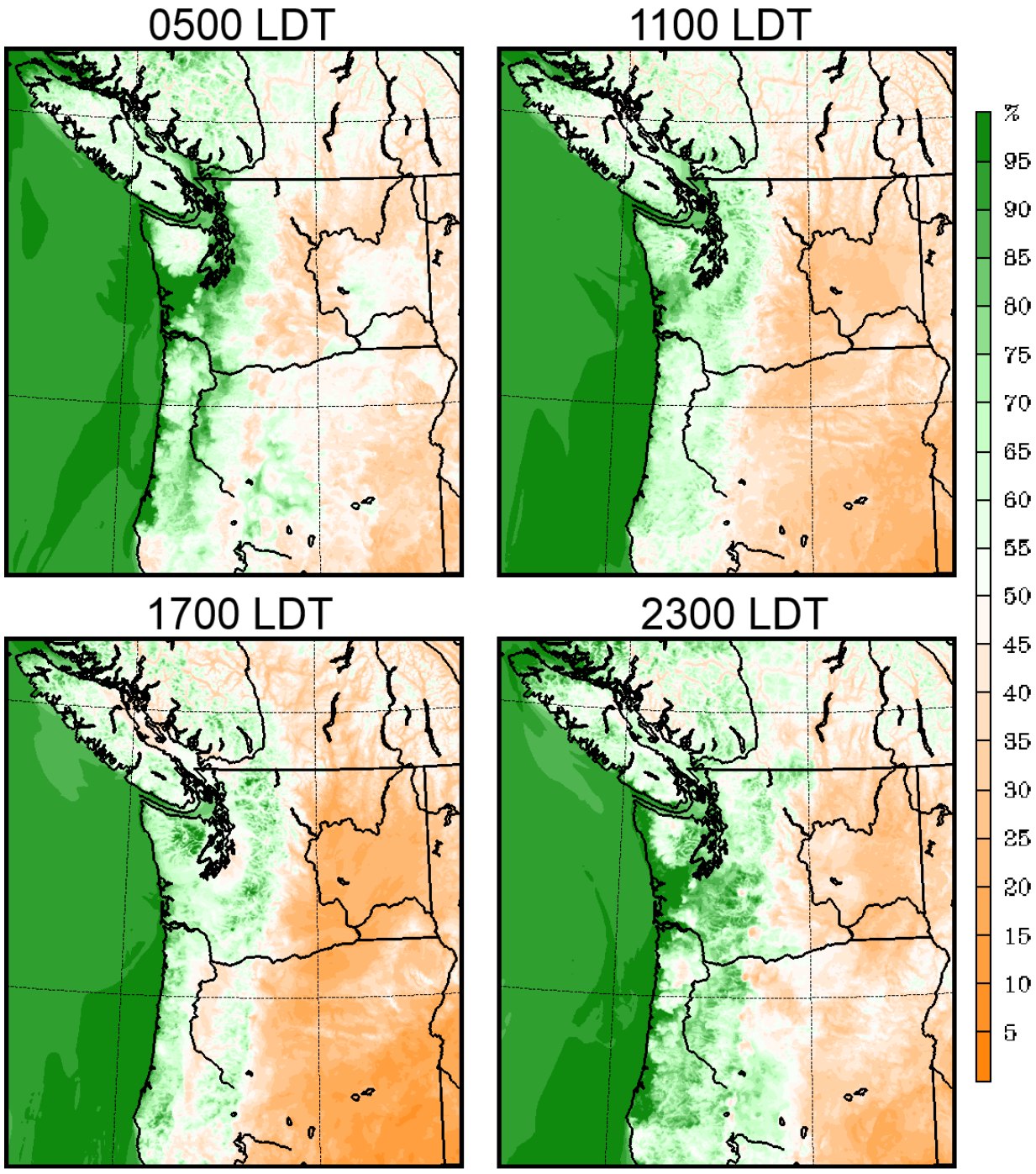

Figure 14: Evolution of 2-m relative humidity from the WRF run.

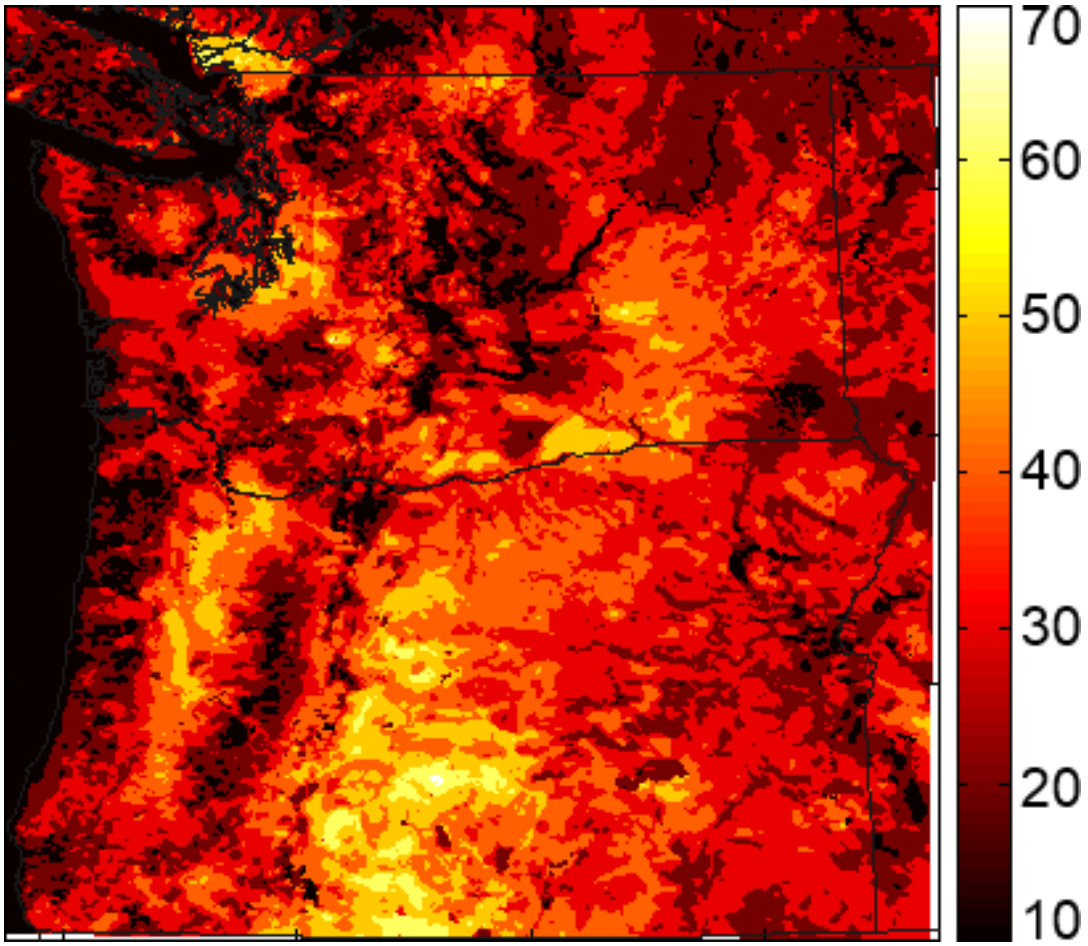

Figure 15: Range of RH in % at 2m.

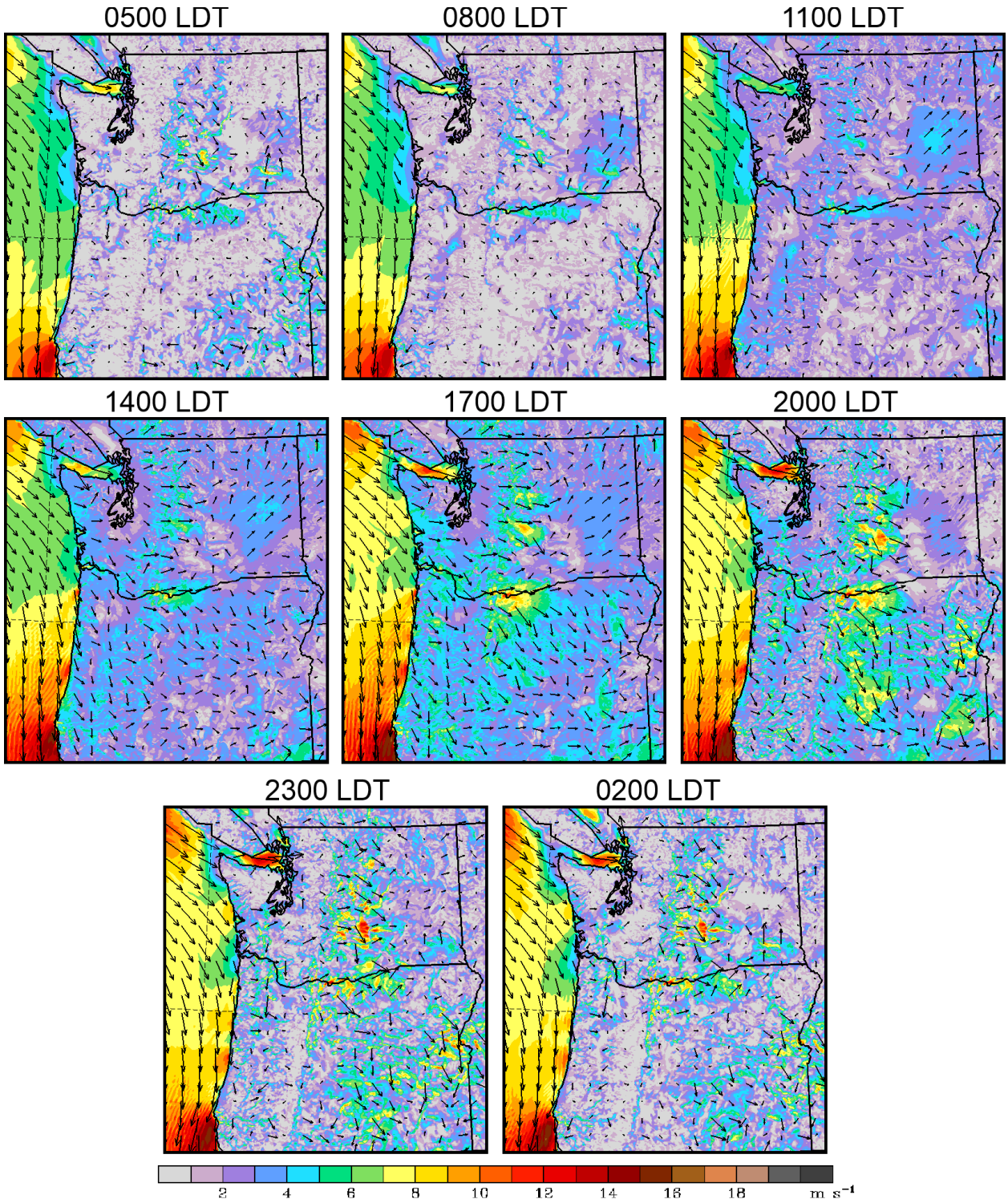

Figure 16: 10-m simulated wind (colors and vectors).

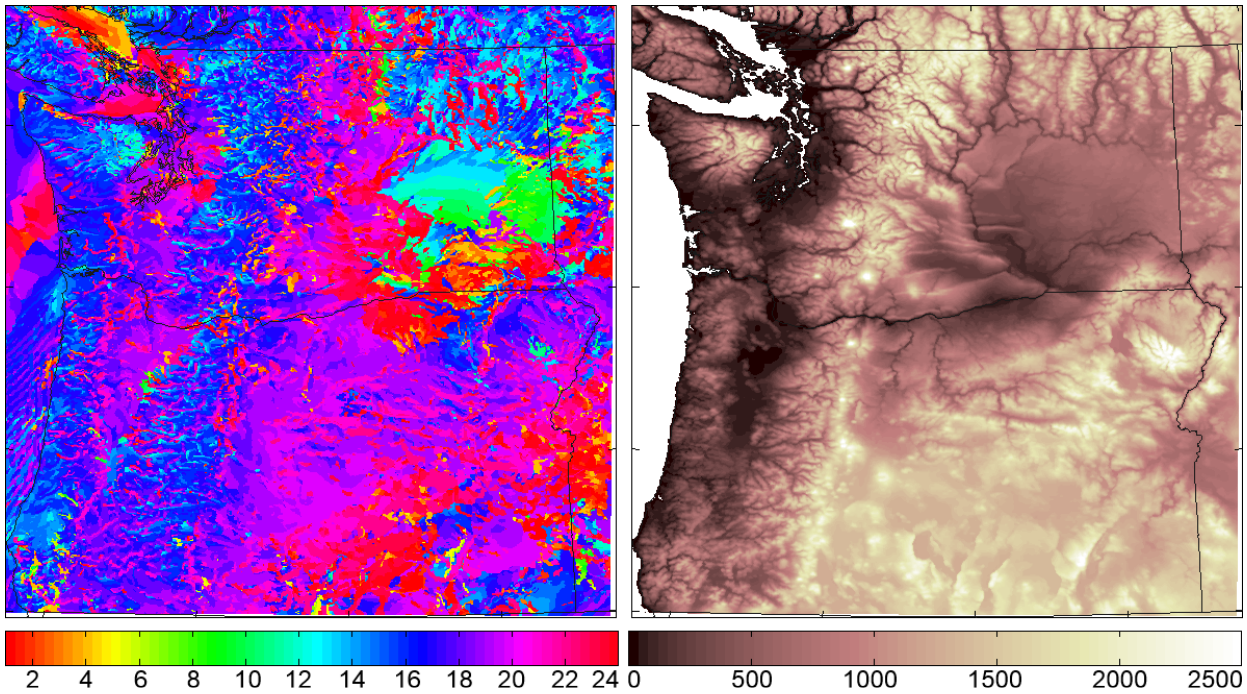

Figure 17: Hour at which the maximum wind is reached (LDT, left), and terrain height (meters, right).

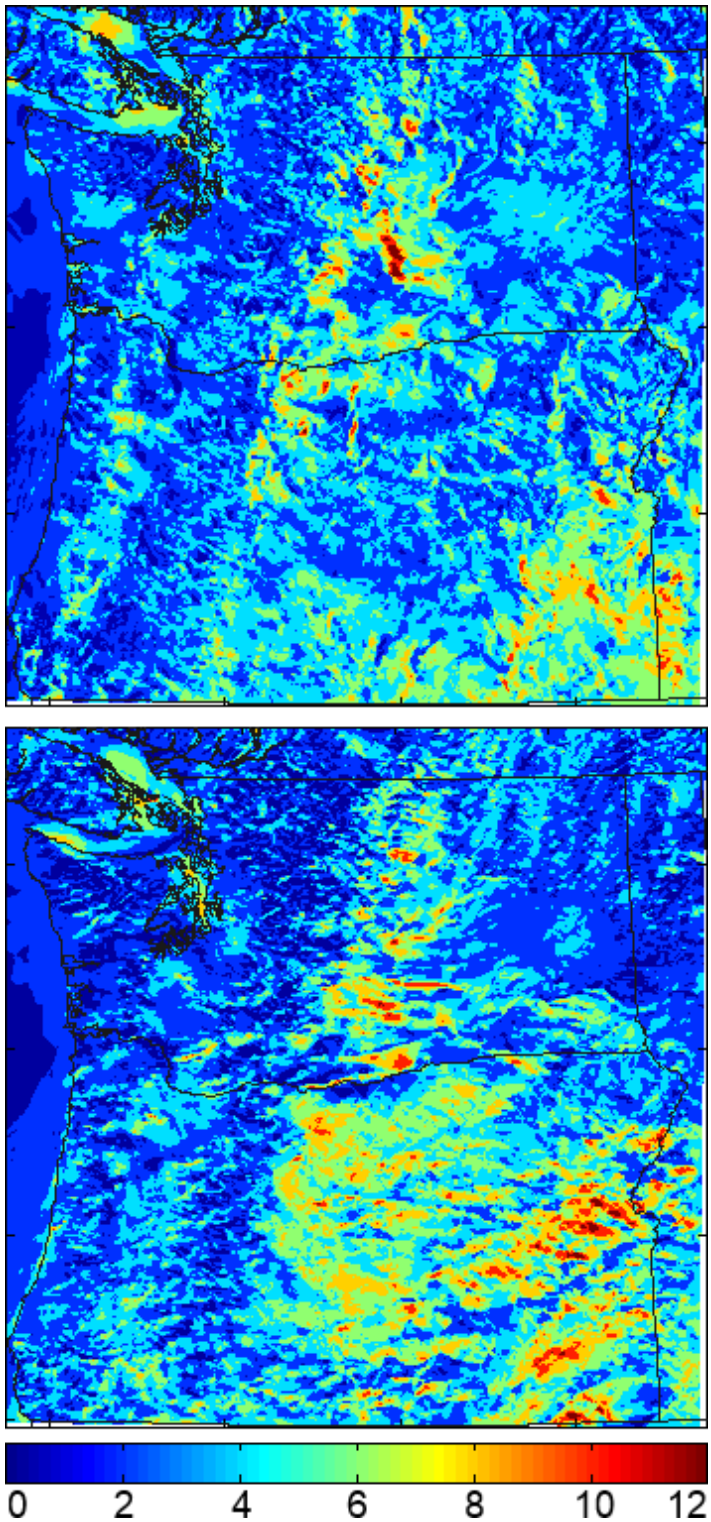

Figure 18: Diurnal range of 10-m u (top) and v (bottom) wind components.

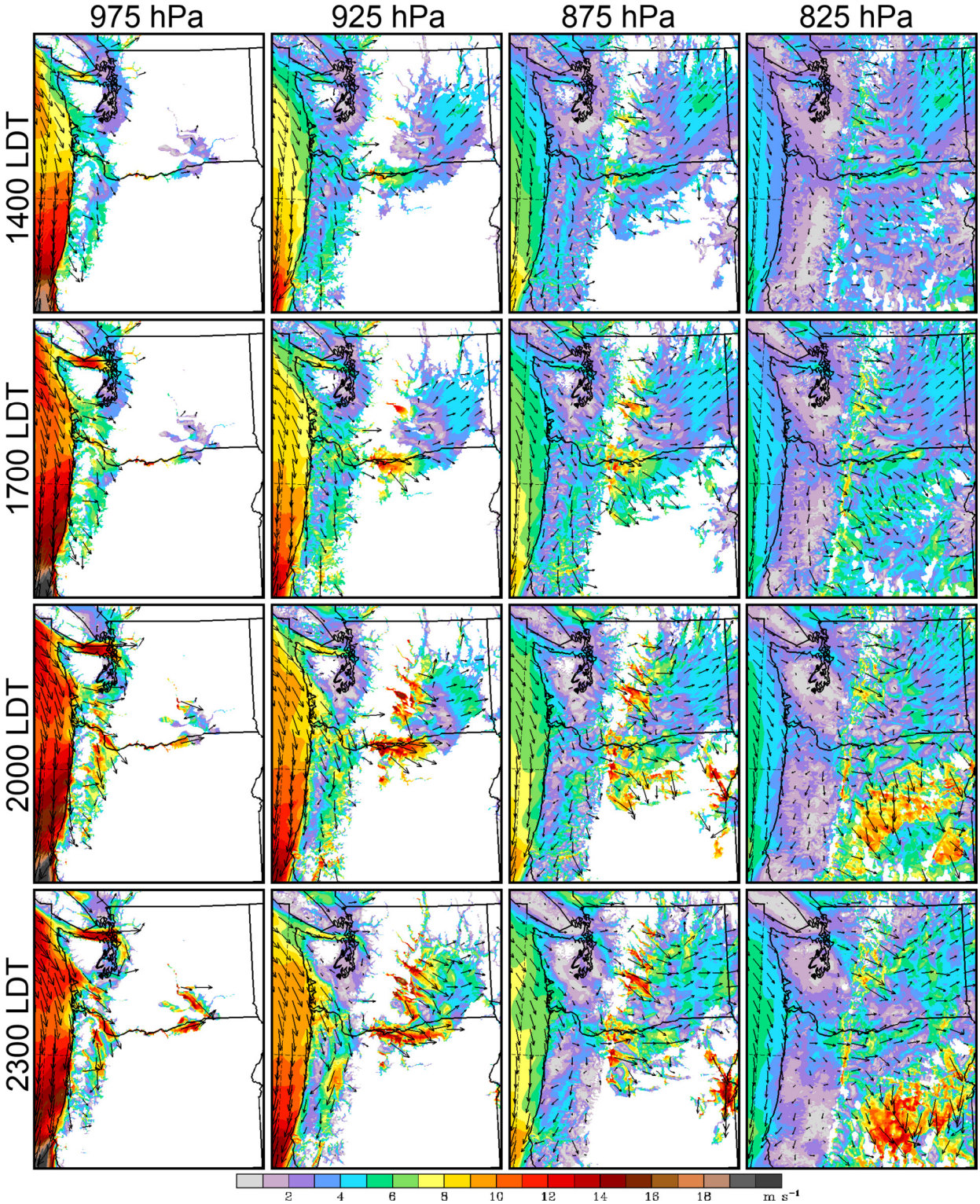

Figure 19: Wind (colors and vectors) with terrain above the pressure level blocked out.

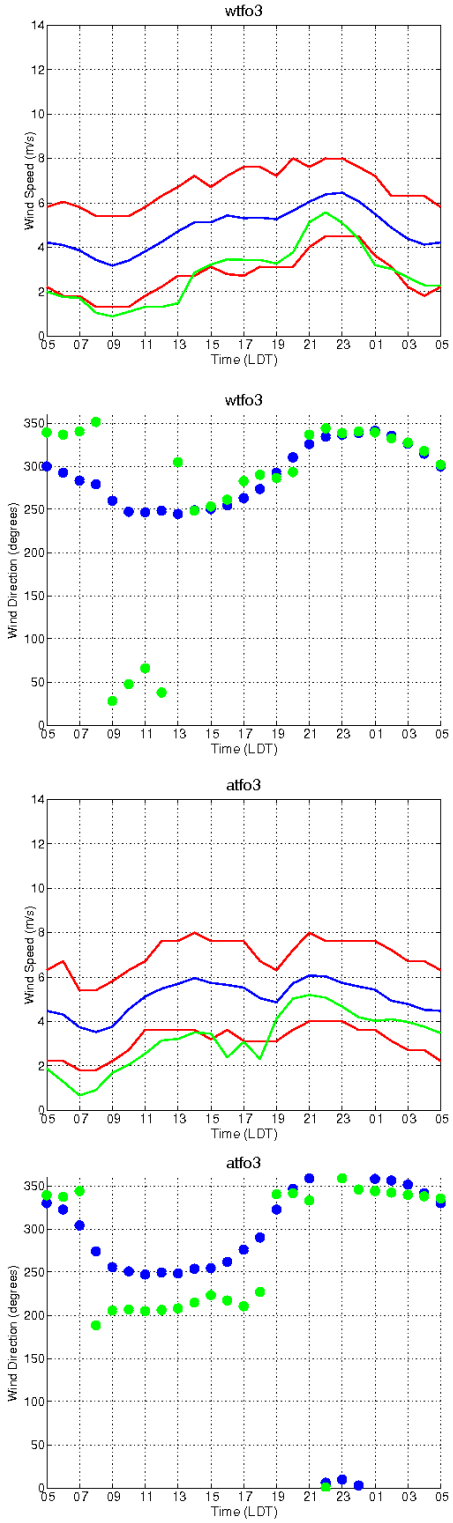

Figure 20: Comparison of model (green) and observational (blue) wind speed and direction. Wind speeds shown as in Figure 7.

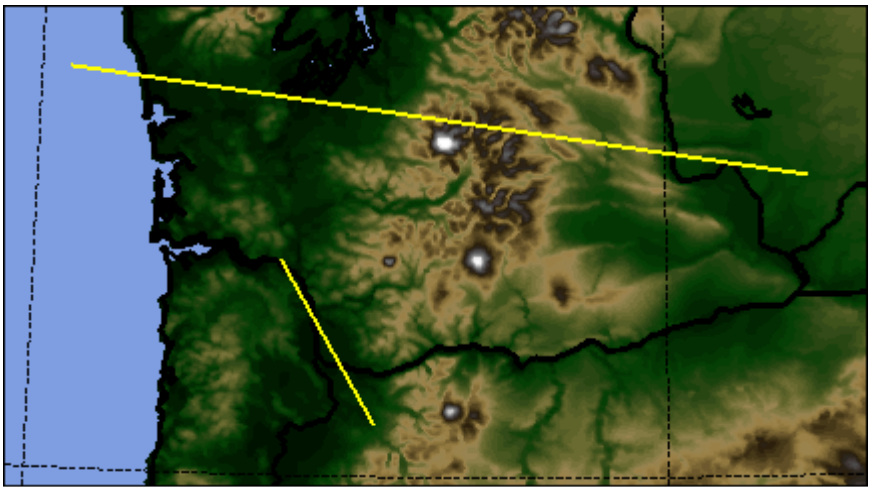

Figure 21: Locations of cross sections for Figures 22 (short yellow line) and 23 (long yellow line).

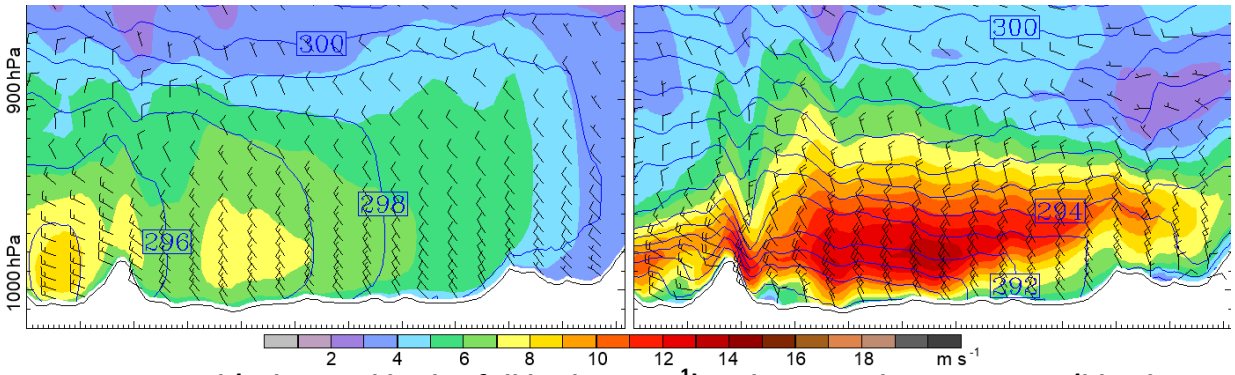

Figure 22: Wind (colors and barbs, full barb=5 m s^{-1}) and potential temperature (blue lines, °K) from the 4/3 km WRF simulation for 1600 (left) and 2200 (right) LDT.

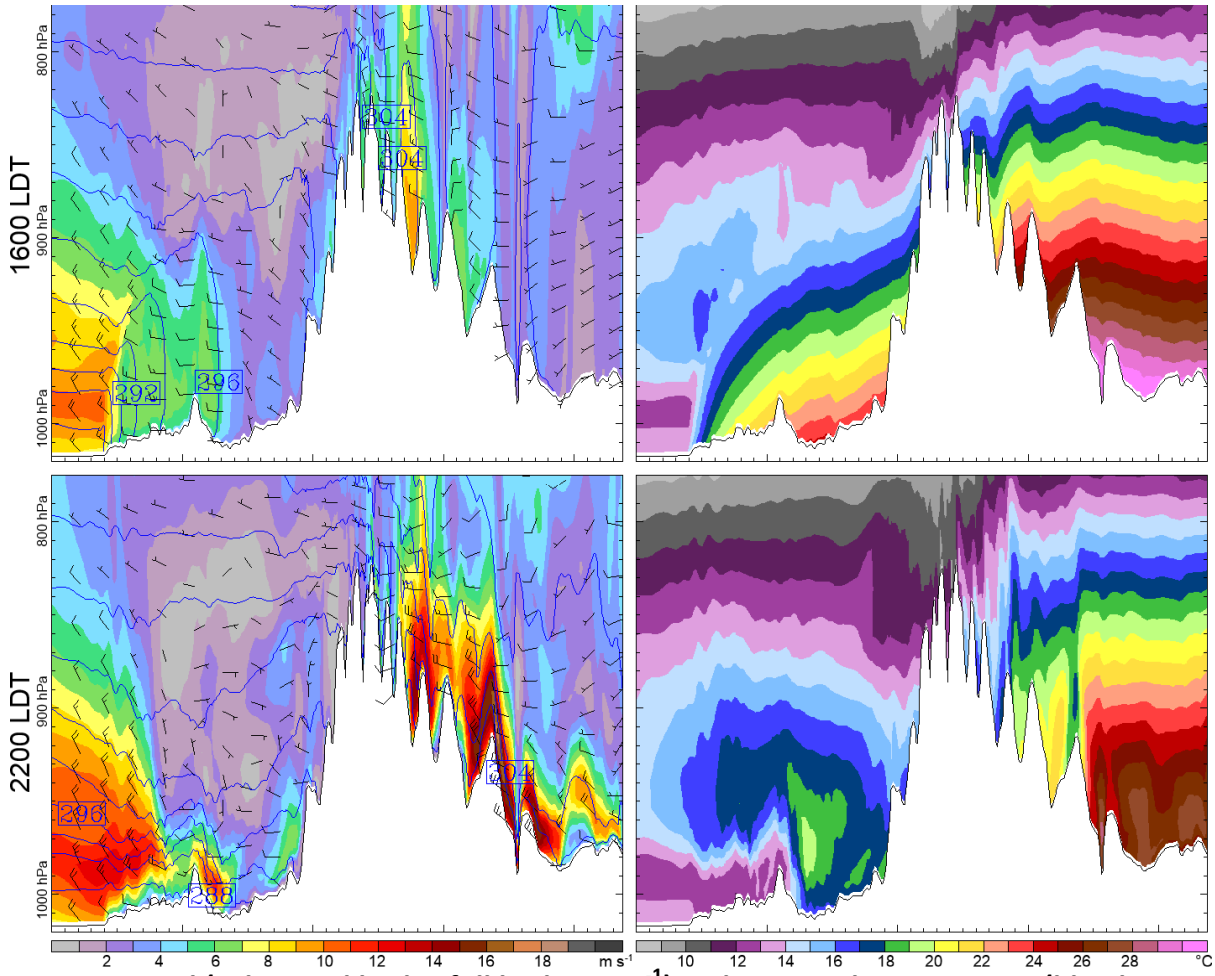

Figure 23: Wind (colors and barbs, full barb=5 m s^{-1}) and potential temperature (blue lines, °K) on the left, and temperature (°C) on the right from the 4/3-km WRF simulation.